

Interaction between volcanism, tectonics and sedimentation in a shallow carbonate platform: A case study from the western Tethys (Middle Jurassic, southeastern Iberian Range)

Interacción entre vulcanismo, tectónica y sedimentación en una plataforma carbonatada somera: Ejemplo en el Tethys occidental (Jurásico Medio, sureste de la Cordillera Ibérica)

J.E. Cortés¹

¹ Departamento de Geodinámica, Estratigrafía y Paleontología, Facultad de Ciencias Geológicas, Universidad Complutense de Madrid. José Antonio Novais 12, 28040 Madrid, Spain. Email: jocortes@ucm.es; ORCID ID: <https://orcid.org/0000-0003-0477-6837>

Corresponding author

ABSTRACT

In the southeastern Iberian Range, several mainly volcanoclastic rocks resulting from submarine eruptions can be found interbedded in the Lower–Middle Jurassic carbonate succession. The geological mapping of the outcropping volcanic rocks reveals that they follow three well marked lineaments of cortical weakness (Teruel, Caudiel and Alcablas Fault Zones), probably caused by the faulting related to the opening and sea–floor spreading of the Ligurian and Alpine Tethys oceans. The present work introduces the results of the study, which aims to evaluate the tectonosedimentary evolution of a shallow submarine setting affected by volcanism during the Aalenian–Bajocian boundary (Middle Jurassic). This site, known as “Caudiel volcanic outcrop”, is located at the southeastern part of the Caudiel Fault Zone. The presence of positive subaqueous volcanoclastic reliefs, added to shallow marine platforms, strongly affects the depth–dependent carbonate sedimentation: it induces substantial changes in lithofacies compared to other neighboring areas, or even directly prevents the sedimentation. Moreover, episodic normal fault activity generated a dynamic topography over time, with variable rates of both subsidence and uplifting throughout different areas. The Caudiel outcrop represents a good ancient example of interaction between multiple factors (volcanism, tectonism and sedimentation) in shallow carbonate platforms, where the accommodation changes and the sedimentation rates seem to be subordinate to the local tectonic disturbances.

Keywords: volcanism; sedimentation; ammonites; paleogeography; Middle Jurassic; Iberian Range.

RESUMEN

En el sureste de la Cordillera Ibérica (España) existen una serie de afloramientos de rocas volcánicas originadas por erupciones submarinas, principalmente de tipo volcanoclástico, interestratificadas en las sucesiones carbonatadas del Jurásico Inferior y Medio. La cartografía geológica de los afloramientos de rocas volcánicas revela que se encuentran alineados a lo largo de tres elementos de debilidad cortical bien definidos (zonas de falla de Teruel, de Caudiel y de Alcablas), originados probablemente por fracturas relacionadas con la apertura

Recibido el 5 de mayo de 2019; Aceptado el 12 de diciembre de 2019; Publicado online el 9 de julio de 2020

Citation / Cómo citar este artículo: Cortés J.E. (2020). Interaction between volcanism, tectonics and sedimentation in a shallow carbonate platform: A case study from the western Tethys (Middle Jurassic, southeastern Iberian Range). *Estudios Geológicos* 76(1): e129. <https://doi.org/10.3989/egeol.43590.537>.

Copyright: © 2020 CSIC. This is an open-access article distributed under the terms of the Creative Commons Attribution-Non Commercial (by-nc) Spain 4.0 License.

y expansión del Tethys Ligur y del Tethys Alpino. En este trabajo se presentan los resultados del estudio de la evolución tectonosedimentaria de un ambiente submarino somero afectado por la presencia de una acumulación volcánica que tuvo lugar en el Jurásico Medio (límite Aaleniano–Bajociano). Se trata del afloramiento volcánico de Caudiel, que es el más suroriental de todos los afloramientos localizados en uno de los tres elementos de debilidad estructural mencionados: la Zona de Falla de Caudiel. La presencia de un relieve positivo en el fondo de la plataforma, ya de por sí bastante somera, condiciona la sedimentación carbonatada, muy sensible a la profundidad, hasta el punto de llegar a inducir cambios significativos de facies con respecto a otras áreas cercanas o de impedir la sedimentación. Los movimientos episódicos del substrato generaron una topografía irregular y cambiante a lo largo del tiempo, con tasas variables de hundimiento y levantamiento en diferentes áreas. El afloramiento de Caudiel constituye un buen ejemplo fósil de interacción entre varios factores (volcanismo, tectónica y sedimentación) en plataformas carbonatadas someras, en las que los cambios de acomodación y las tasas de sedimentación parecen estar subordinadas a perturbaciones tectónicas de carácter local.

Palabras clave: vulcanismo; sedimentación; ammonites; paleogeografía; Jurásico Medio; Cordillera Ibérica

Introduction

After the Permian–Triassic rifting interval, Iberia evolved into a passive margin stage from the latest Triassic until the end of the Middle Jurassic. Meanwhile, active rifts were taking place both in the west (leading to the onset of spreading in the northern part of the Central Atlantic Ocean), and in the south and east (resulting in the generation of the Ligurian and Alpine Tethys Oceans) of Iberia (Gómez et al., 2019) (Fig. 1). Middle Jurassic sedimentation in the eastern margin of Iberia took place on a carbonate–platform system in which the accumulation rate, thickness and lithofacies were controlled by a grid of NW and NE active faults. These faults differentiated blocks with variable subsidence rates conforming paleogeographic highs and depocenters, as well as internal and external platform facies types (Fernández–López & Gómez, 1990, 2004; Gómez & Fernández–López, 2004a, 2006; García–Frank, 2006; García–Frank et al., 2006, 2008; Gómez et al., 2019) (Fig. 1B). It can be intuited that NW–SE trending faults run virtually parallel to transform faults formed during the opening of the Ligurian Tethys Ocean (transtensional faulting), while the NE–SW trending faults seem to be following the trend of the extensional faulting system related to sea–floor spreading (Gómez et al., 2019). Jurassic active volcanism was restricted to the southeasternmost areas of the eastern Iberian platform system. However, the volcanic outcrops have been found closely circumscribed to the tracks of the NW (Caudiel and Alcublas Fault Zones) and NE (Teruel Fault Zone) trending major faulting, and they appear conspicuously located where the two orthogonal fault systems intersect (Fig. 1B). Volcanic rocks result from subaqueous volcanic eruptions that occurred throughout the early Pliensbachian–early

Bajocian interval (Cortés, 2018), so we are facing a magma–rich episode within the Early Passive Margin Stage from the Alpine Cycle (Gómez et al., 2019). Biostratigraphic methods have been applied to quantify and date the Jurassic volcanic phases in the southeastern Iberian Range. Several thousands of ammonites and brachiopods were subjected to taxonomic and taphonomic analyses, revealing 13 individual and time–successive volcanic phases from the early Pliensbachian to the early Bajocian (Cortés, 2018). The Caudiel volcanic outcrop (Fig. 2A) includes two volcanic phases, the most recent being the subject of this study. It coincides in time with the Concavum–Discites chronozone boundary (Cortés & Gómez, 2016; Cortés, 2018), and corresponds to the 12th position of the total (Cortés, 2018) (Fig. 2B). Today, the section exposed of the volcanic rocks is estimated to be about 3 km long in an approximately N–S direction, and about 50 m wide in its maximum thickness, in the middle–north part of the mound.

The first studies dealing with Middle Jurassic volcanics in the Caudiel outcrop were carried out by Ortí & Sanfeliu (1971), Gómez & Goy (1977), Gómez (1979), Ortí & Vaquer (1980), and Fernández–López et al. (1985). From all the authors mentioned, the work performed by Gómez (1979) is particularly noteworthy. The author described 26 stratigraphic logs that were distributed across the northern part of the volcanic structure (Fig. 3) to demonstrate that the flank of the volcanic mound was progressively overlapped by Bajocian, Bathonian and Callovian carbonate beds.

Similar cases, of both the same and different ages, where tectonism and volcanic accumulations influence the sedimentary infill, were cited by Vera et al. (1997) in the Betic Cordillera (southern Spain), or by Santisteban (2016, 2018) in the Iberian Range (southeastern Spain).

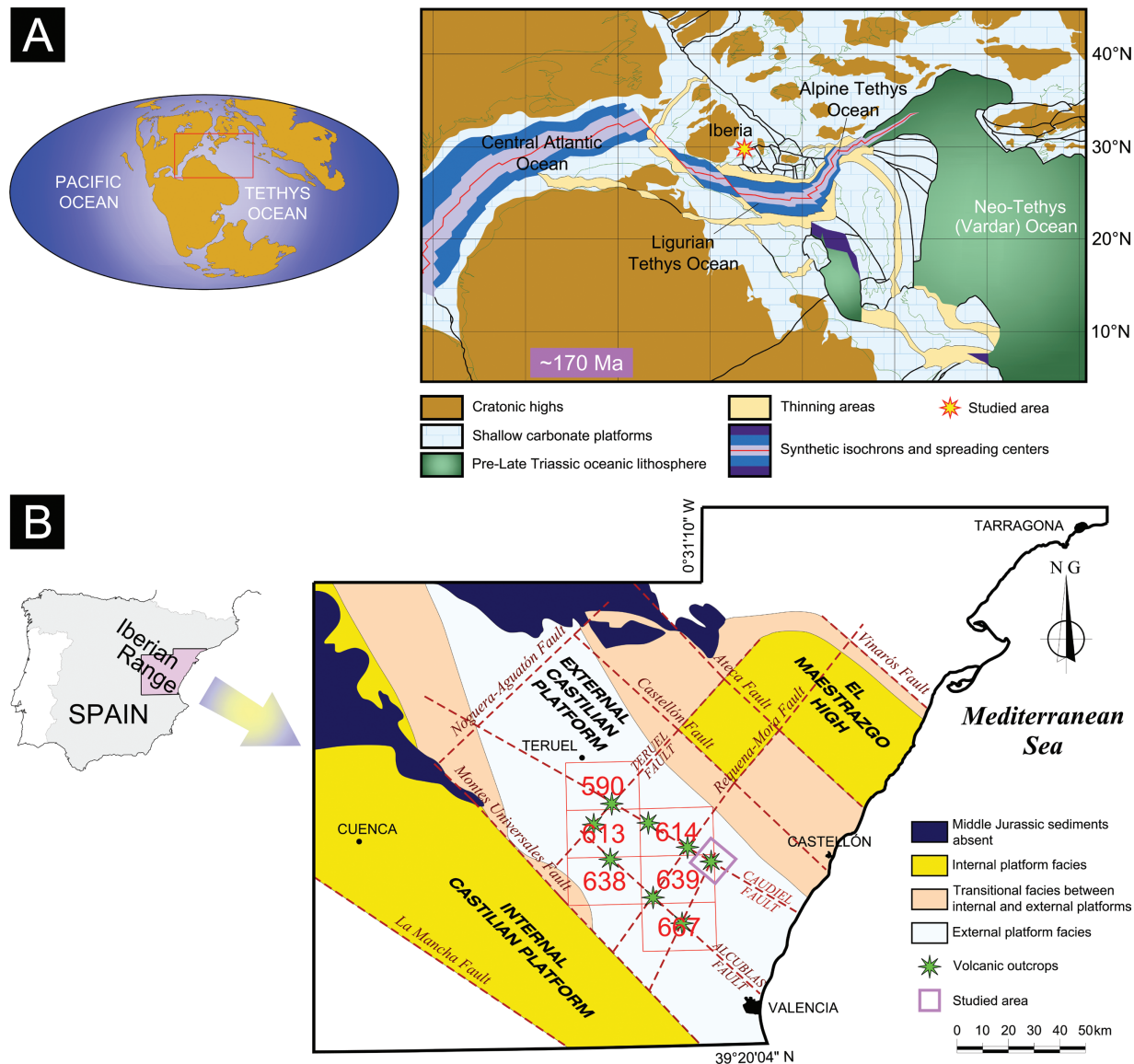


Figure 1.—Location of the studied area. **A**) Middle Jurassic (~170 Ma) paleogeography of Western Tethys Ocean, with location of Iberia and the studied area, modified after Ziegler (1990), Stampfli & Borel (2002, 2004), Stampfli et al. (2002), Stampfli & Hochard (2009), Osete et al. (2011) and Schettino & Turco (2011). **B**) Paleogeographical reconstruction of the carbonate-platforms system developed in the Iberian Basin during the Middle Jurassic. The distribution of paleogeographic elements, strongly controlled by a netting of synsedimentary faults, the location of volcanic deposits and the studied area are also indicated. Modified after Gómez & Fernández-López (2006) and Gómez et al. (2019). Sheets of the Geological Map of Spain at the scale of 1:50,000: 590 [La Puebla de Valverde] (Adrover et al., 1983), 613 [Camarena de la Sierra] (Abril et al., 1978), 614 [Manzanera] (Gautier, 1974), 638 [Alpuente] (Abril et al., 1975), 639 [Jérica] (Campos et al., 1977) and 667 [Villar del Arzobispo] (Lazuen & Roldán, 1977).

Since it is possible to investigate the tectonic controls of a given region by analyzing the changes in the sedimentary infill (e.g. McCann & Saintot, 2003), the present work focuses on reconstructing the architecture of a shallow marine carbonate succession affected by explosive volcanism in order to reveal its tectosedimentary evolution. To achieve this goal,

the following performances have been carried out: (1) to take up again and revise the area previously studied by Gómez & Goy (1977), Gómez (1979) and Fernández-López et al. (1985), (2) to expand the research much farther northward from the end of the volcanic deposits, (3) to complete the stratigraphic, chronostratigraphic and sedimentological study of

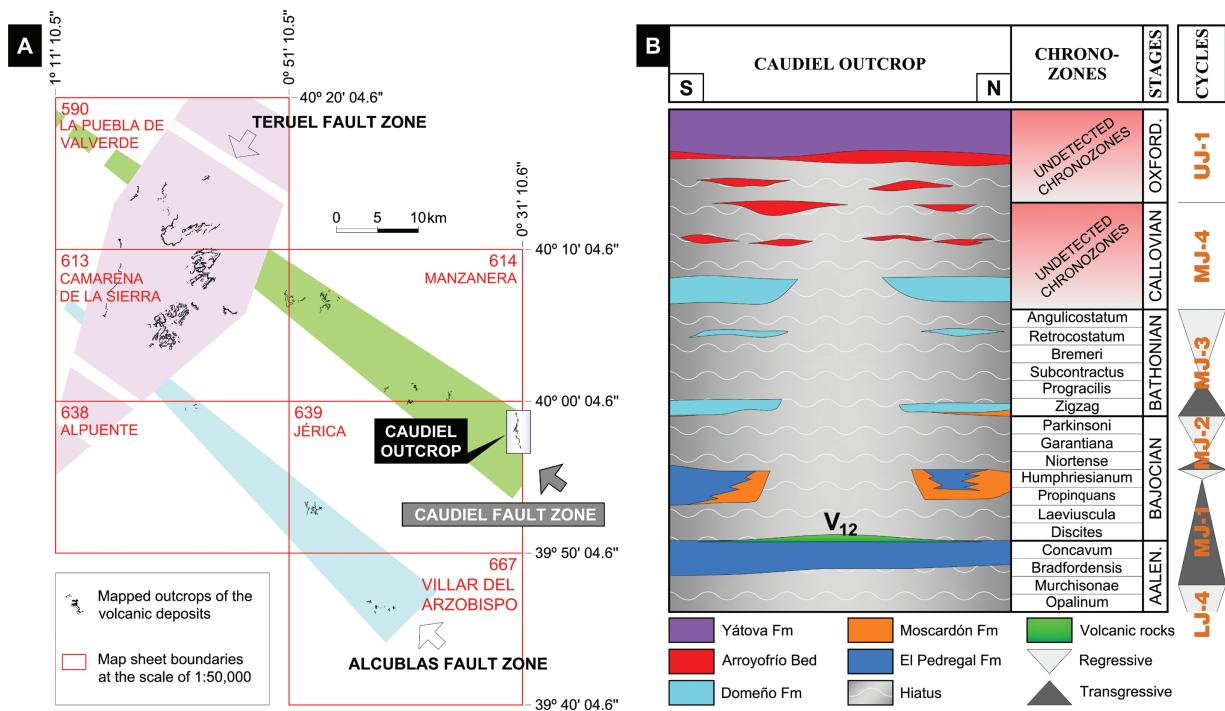


Figure 2.—Regional location and stratigraphy of the Caudiel volcanic outcrop. **A)** Caudiel outcrop location in the southeastern tip of NW trending Caudiel Fault Zone. Remaining outcrops fall outside the scope of this work. Exposed volcanic rocks are included into 6 sheets of the Geological Map of Spain at the scale of 1:50,000 (see Fig. 1). The Caudiel outcrop lies into the sheet 639 [Jérica] (Campos et al., 1977). **B)** Stratigraphic chart showing the volcanic level (V_{12}), the lithostratigraphic units and the cycles of the Middle Jurassic in the Caudiel outcrop over a time frame. Note that the lithostratigraphic units (El Pedregal and Moscardón Formations) have been drawn with no lateral continuity in the central parts of the Caudiel outcrop. These units are onlapping the flanks of the volcanic mound formed at the onset of the Bajocian.

post-volcanic carbonate sediments over the southern flank of the volcanic building.

Stratigraphical remarks

The typical Middle Jurassic lithostratigraphic units of the Chelva Group (El Pedregal, Moscardón and Domeño Formations, together with Arroyofrío Bed) show particular features in the area under study, due to the presence of the Caudiel volcanic mound. The El Pedregal Formation consists of bioclastic wackestone–packstone limestones, the Moscardón Formation is formed by crinoidal packstone–grainstone or grainstone limestones, the Domeño Formation is composed of bioclastic (microfilaments) wackestone–packstones, and the Arroyofrío Bed is made up of wackestone–packstones bearing ferruginous ooids and pisoids. The El Pedregal and Domeño Formations, as well as the Arroyofrío Bed, are shown as units with ammonite chronozone biostratigraphic resolution. However, ammonites

are extremely scarce or absent in the high-energy and wave-dominated Moscardón Formation (Fernández-López et al., 1985; Fernández-López & Gómez, 2004; Gómez & Fernández-López, 2004a, 2006; Cortés, 2018).

In the El Pedregal Formation, the ammonites identified the Bradfordensis and Concavum chronozones of the late Aalenian, and the Propinquans and Humphriesianum chronozones of the early Bajocian. Therefore, the Aalenian Murchisonae Chronozone, Discites and Laeviuscula chronozones of the early Bajocian, and the whole late Bajocian correspond to local stratigraphic gaps (Fig. 2B) (Fernández-López et al., 1985; Cortés, 2018). The most basal layers of the Moscardón Formation have provided typical specimens of the Bathonian Zigzag Chronozone (Fernández-López et al., 1985; Fernández-López, 1986). Nevertheless, in the northernmost part of the Caudiel outcrop, grainstone limestones attributable to the Moscardón Formation interfinger southward with their time-equivalent

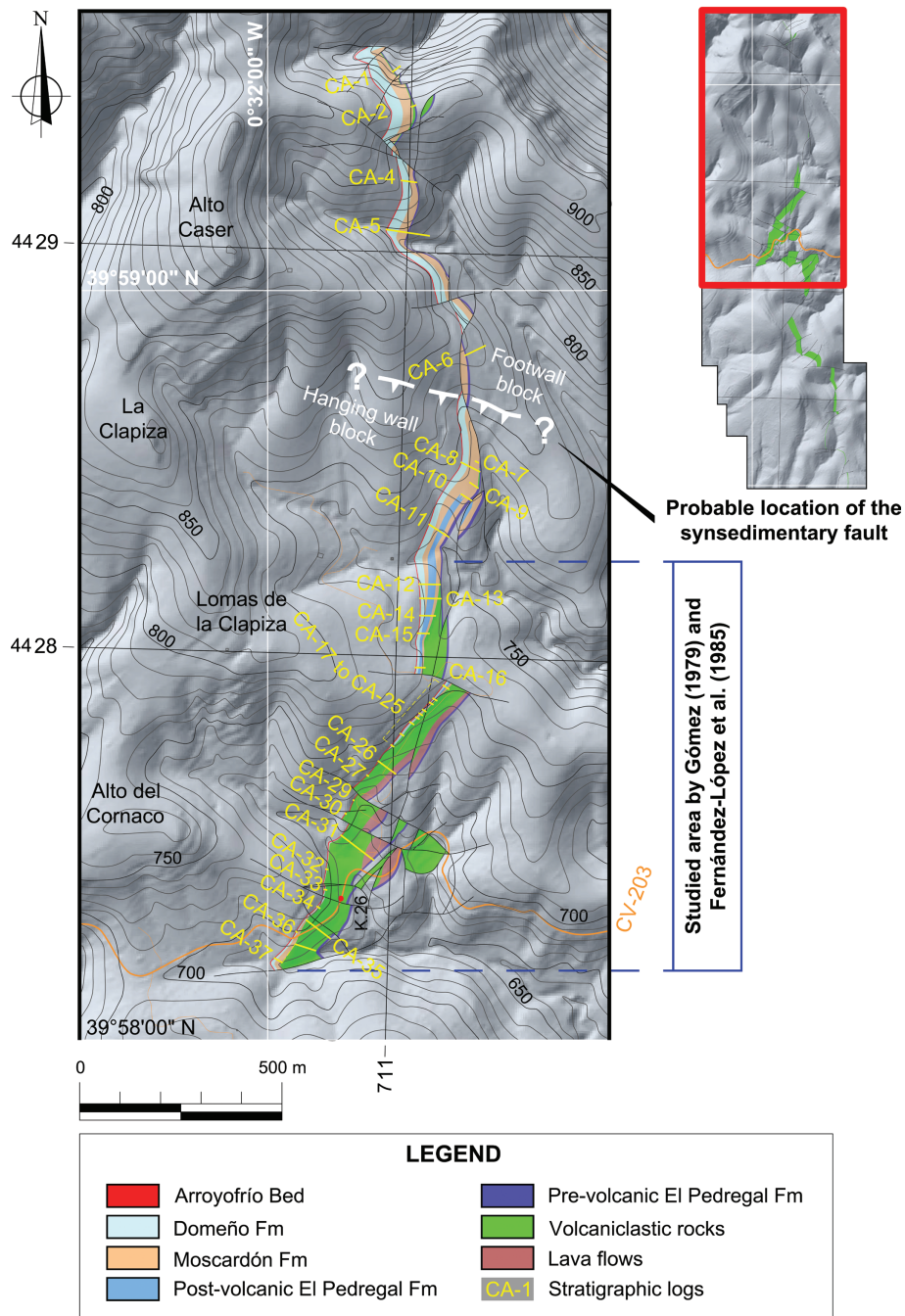


Figure 3.—Geological mapping (northern part) including volcanic deposits and lithostratigraphic units of the Middle Jurassic (El Pedregal, Moscardón, Domeño Formations and Arroyofrío Bed). Note that post-volcanic El Pedregal Fm is absent in the northernmost part of the map. This is because Bajocian lithofacies B and C have been included within the Moscardón Formation.

Propinquans–Humphriesianum finer wackestone–packstone limestones of the El Pedregal Formation (Fig. 2B) (Cortés, 2018). Except for the Zigzag Chronozone, present again in the lower half of the Domeño Formation, a new stratigraphic gap spans

virtually all the middle and late Bathonian. The ammonoids obtained from the upper half of the Domeño Formation indicate a Callovian age, but they are not chronozonally diagnostic (Fig. 2B) (Cortés, 2018).

Materials and methods

The study of the Middle Jurassic volcanic phase in the Caudiel outcrop has been basically accomplished from field work (Cortés, 2018). A detailed geological mapping of the volcanic and surrounding sedimentary rocks was performed, together

with the measurement of 65 stratigraphic logs, ordered and N–S equidistantly distributed along the outcropping volcanic accumulation (Figs. 3, 4). Field sedimentological descriptions were complemented and supported by 21 thin sections of the main lithofacies examined under the petrographic microscope.

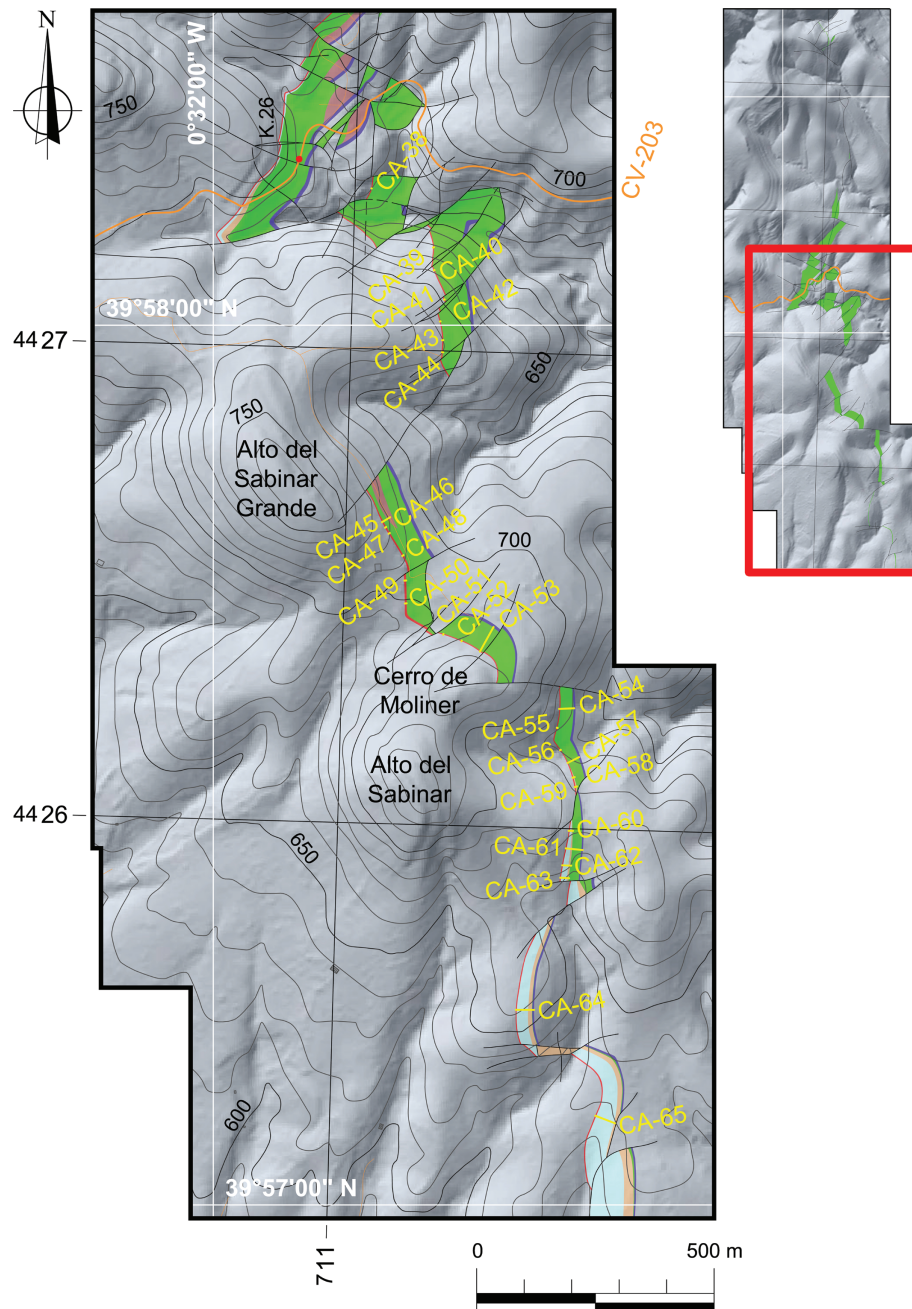


Figure 4.—Geological mapping (southern part) including volcanic deposits and lithostratigraphic units of the Middle Jurassic (El Pedregal, Moscardón, Domeño Formations and Arroyofrío Bed).

Based on 500 ammonite specimens extracted from the carbonate strata, taxonomic and taphonomic analyses were carried out by Professors Fernández-López and Ureta (Departamento de Geodinámica, Estratigrafía y Paleontología, Facultad de Ciencias Geológicas, Universidad Complutense de Madrid) in order to date the pre-volcanic sediments, the volcanic phase and the post-volcanic carbonate sediments that interact with the volcanic level. All the taxonomic and taphonomic data are available in Cortés (2018), Cortés et al. (2009) and Cortés & Gómez (2016). Following Fernández-López (1984a,b), resedimented and reelaborated specimens have been distinguished according to their state of preservation. Resedimented ammonoids (transported within the same bed) are represented in the text by the letter (r), whereas the letter (w) is used to identify the reelaborated ones; that is, those reworked from older beds. The biostratigraphical results have been referred to the standard chronozones of the Middle Jurassic in Europe (Callomon, 2003) with the following exceptions: (1) the Ovalis Chronozone has been included as a subchronozone of the Laeviuscula Chronozone according to Fernández-López (1985), (2) the Propinquans Chronozone has been preferred to the Sauzei Chronozone following the guidelines of Fernández-López & Mouterde (1994) and Fernández-López (1997a,b), (3) the Niortense Chronozone was used instead of the Subfurcatum Chronozone, in agreement with Fernández-López & Mouterde (1994) and Fernández-López (1997a,b). Chronozonal nomenclature used in this work meets the lines of Page (2003) and Callomon (2003). This nomenclature is accepted by the International Subcommission on Jurassic Stratigraphy, at least when applied to Jurassic ammonoids.

The lithostratigraphic units have been taken from the works of Gómez & Goy (1979) and Gómez & Fernández-López (2004b). The sedimentary cyclicity utilized in this work is the one established by Fernández-López (1997a,b), Aurell et al. (2003), Fernández-López & Gómez (2004) and Gómez & Fernández-López (2004a, 2006).

Results

The authors mentioned above have defined four second-order cycles during the Middle Jurassic on the Iberian carbonate platform system: MJ-1, MJ-2,

MJ-3 and MJ-4 (Fig. 2B). In the Caudiel outcrop, it has been possible to recognize the four cycles with a different degree of development and with long breaks in sedimentation.

The MJ-1 second-order Cycle

The MJ-1 Cycle (Murchisonae p.p. Chronozone – end of the Humphriesianum Chronozone) is represented by the lower and middle part of the El Pedregal Formation.

Pre-volcanic sediments

Pre-volcanic sedimentation in the MJ-1 Cycle started with grayish to reddish bioclastic wackestone-packstone limestones, 2 m thick in their maximum thickness, which contain occasionally phosphatic or ferruginous oolites and usually firmgrounds or hardgrounds developed at the top of beds that present signs of bioturbation (*Thalassinoides*). Resedimented and reelaborated ammonite specimens have enabled the identification of the Bradfordensis and Concavum chronozones (*Brasilia* sp., *Apedogyria* sp., *Vacekia* sp., *Erycites* sp., *Abbasitoides* sp., *Abbasites* sp., *Rodaniceras* sp., *Graphoceras* sp., *Ludwigella* sp.). No specimens belonging to the Murchisonae Chronozone in the El Pedregal Formation have been found.

Volcanic deposits

Volcanic rocks were emplaced on the carbonate platform at the early stages of the MJ-1 Cycle, overlying the Aalenian (Concavum Chronozone) limestones. The volcanic products consist almost exclusively of explosive volcanoclastic deposits with abundant clasts of sedimentary rocks, although effusive lavas may be a minority component. Lava flows (Fig. 5A) grade vertically and laterally into volcanoclastic deposits (Fig. 5B), which, in turn, pass laterally into epiclastic accumulations. Here the term ‘volcanoclastic’ is used as a descriptive term for fragmental volcanic rocks with no genetic implications, and the term ‘epiclastic’ is used when post-eruptive sedimentary activity can be identified with certainty. Lava lobes coincide with, or are near to, the maximum thickness of the mound; however, feeder dykes linked to vent sites have not been found.

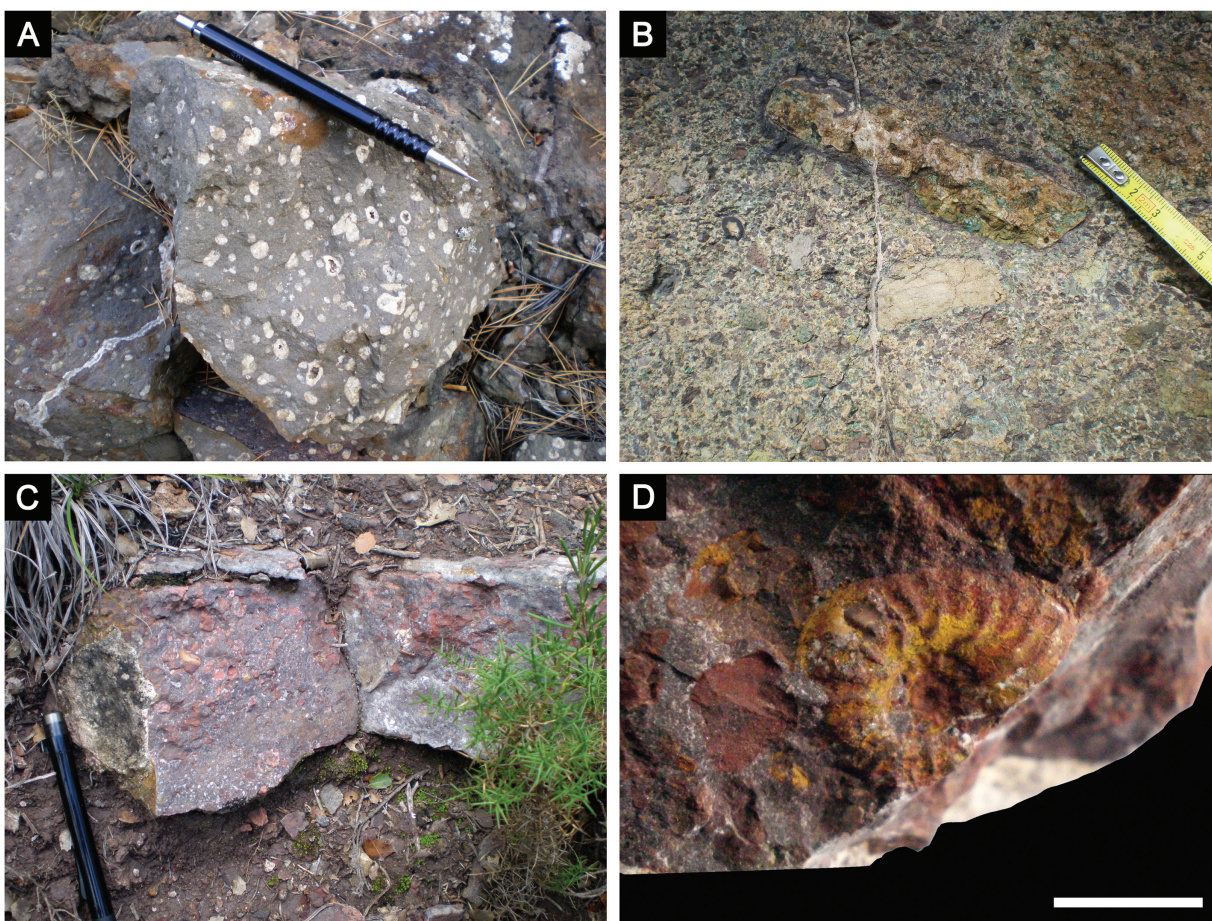


Figure 5.—Field photographs. **A)** Lava flows in level 13 of CA–31 stratigraphic log. **B)** Volcaniclastic rocks in level 37 of CA–35 stratigraphic log. **C)** Intervolcanic bed in level 3 of CA–12 stratigraphic log. **D)** *Ludwigella* sp. (w) from the intervolcanic bed in level 3 of CA–12 stratigraphic log. Pencil for scale in A) and C) is 14 cm length. Scale bar in D) corresponds to 1 cm.

Post–volcanic sediments

The post–volcanic carbonate sediments present variable thicknesses that range from 0 on the volcanic flanks up to a maximum of 20 m in CA–12 stratigraphic log. Three main types of carbonate lithofacies from the El Pedregal Formation are identified in the post–volcanic succession during the early Bajocian MJ–1 Cycle, based on field observations (grain size, bedding characteristics or sedimentary structures) and petrographic analysis (texture, allochem types). These lithofacies are: A) bioclastic wackestone–packstone limestones, B) crinoidal wackestone to grainstone limestones, and C) Cross-bedded bioclastic grainstone limestones.

Lithofacies A is a grayish bioclastic wackestone–packstone with centimetric to decimetric irregular

chert nodules (Fig. 6A) and abundant macrofossils of cephalopods (belemnites and ammonites). Under petrographic microscope, it shows a mud– to grain–supported fabric with sectorally packed allochems embedded into a micritic to microsparitic, even pseudosparitic, matrix (Fig. 6B). Skeletal grains are basically composed of echinoderm fragments (almost all of them crinoids), minor thin–shelled (microfilaments) and thick–shelled bivalves, punctate brachiopods, foraminifera, bryozoans, ostracods, and serpulids. Non–skeletal grains consist of rounded to subangular intraclasts and peloids of different sizes, as well as fine subhedral or anhedral crystals of terrigenous quartz (<1%). Blocky sparry cement is occasionally present inside intergranular voids, whereas syntaxial overgrowth cements on echinoderm plates are very common. Silicification is

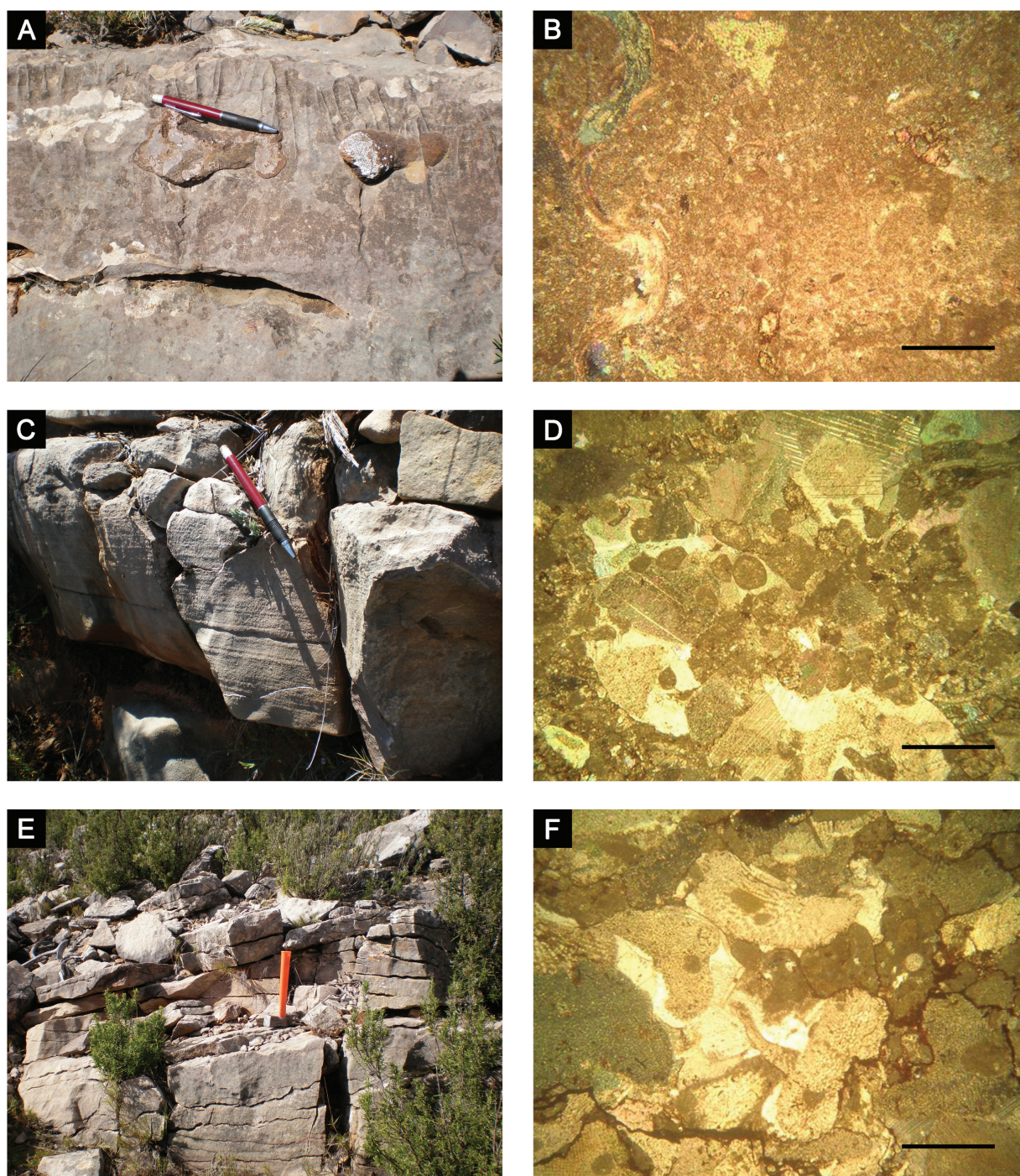


Figure 6.—Lithofacies photographs of post-volcanic Bajocian sedimentary rocks on the northern flank. **A)** Field photograph of wackestone–packstone limestones with irregular chert nodules (lithofacies A) in level 19 of CA–13 stratigraphic log. **B)** Microphotograph of lithofacies A, including plates of echinoderms and fragments of thick-shelled bivalves. **C)** Field photograph of massive coarse-grained wackestone to grainstone limestones (lithofacies B) in level 5 of CA–8 stratigraphic log. **D)** Microphotograph of lithofacies B. Bioclasts are almost exclusively plates of echinoderms with overgrowths formed in optical continuity (syntaxial rims). Rounded micritic intraclasts are also common. **E)** Field photograph of cross-bedded bioclastic grainstone limestones (lithofacies C) in level 18 of CA–5 stratigraphic log. **F)** Microphotograph of lithofacies C. Bioclasts, mainly crinoid plates, and irregular-shaped intraclasts show a close packing. Stylolite seams produce an almost nodular fabric. Hammer and pencil for scale are respectively 27 and 14 cm length. Scale bars in B), D) and F) correspond to 500 μm . Cross-polarized light in all the microphotographs.

manifested both by partial silica replacement of thick-shelled bivalves and intergranular microcrystalline aggregates of authigenic quartz.

The thin-bedded to thick-bedded lithofacies A (ranging from 5 to 80 cm) is organized into thickening-, coarsening- and shallowing-upwards sequences, showing remobilization surfaces with reworked ammonites (both resedimented and reelaborated) in the uppermost beds. Firmgrounds and hardgrounds with biogenic trace fossils (usually *Thalassinoides*) and ferruginous crusts are common across the sequence boundaries. Resedimented ammonoid taxa collected from lithofacies A have allowed the recognition of the Propinquans and Humphriesianum chronozones: *Bradfordia* sp., *Nannina* sp., *Dorsetensia* sp., *Strigoceras* sp., *Emileia* sp., *Stemmatoceras* sp., *Itinsaites* sp., *Stephanoceras* sp., *Normannites* sp., *Oppelia* sp., *Skirroceras* sp., *Paulostephanus* sp., *Chondroceras* sp., *Poecilomorphus* sp., *Teloceras* sp.

Lithofacies B is a grayish to bluish gray massive and, normally, coarse-grained wackestone to grainstone with no internal structure or faintly laminated (Fig. 6C). The petrographic microscope reveals a mainly bioclast-supported and densely packed fabric. Microcrystalline micritic matrix is scarce, scattered, and sometimes appears as a fine-bioclastic micrite. Patchy recrystallization of micrite to microspar and even to pseudospar is frequent (Fig. 6D). Skeletal allochems consist almost entirely of fragmented crinoids and, less commonly, fragmented thick-shelled bivalves, punctate brachiopods or foraminifera. Non-skeletal allochems, which are variously sized and shaped, are composed of partly recrystallized micritic intraclasts, very abundant rounded or ellipsoidal mud peloids, and subhedral or anhedral crystals of terrigenous quartz characterized by undulose extinction. Primary intergranular porosity was reduced both by syntaxial overgrowth cement on crinoid fragments and intergranular or shelter inequant blocky mosaics. Cement rims of bladed calcite crystals can also be seen coating shells fragments.

The thick-bedded (up to 2 m thick) massive lithofacies B shows sedimentary structures such as erosional surfaces within beds and occasionally a faint tractive lamination. Bioturbated (*Thalassinoides*) and early cemented firmgrounds/hardgrounds are

developed at the top beds, which are around 1 m thick, whereas more massive and thicker intervals of lithofacies B, with no hardground surfaces, do not show a clear cyclic organization. Moreover, centimetric and sharp-based episodes of lithofacies B can also appear interbedded within the thickest (decimetric) beds of lithofacies A.

Although belemnites are common, the ammonite content is virtually absent in this coarse-grained lithofacies. However, Fernández-López et al. (1985) identified the Propinquans Chronozone in their CAUDIEL-XXVI stratigraphic log, in a lenticular bed with a maximum thickness of 0.5 cm located immediately above the Aalenian beds, based on the presence of *Skirroceras* sp. and *Kumatostephanus perjukundus*.

Lithofacies C is a grayish to reddish gray cross-bedded bioclastic grainstone (Fig. 6E). The microfacies analysis shows a grain (bioclast)-supported fabric with very closely packed grains and absent micritic matrix. Blocky and syntaxial rim calcite cements infill the scarce primary intra-particle porosity (Fig. 6F). The most common bioclasts are fragmented crinoids (plates and stems) and thick-shelled bivalves, with lower percentages of prismatic bivalve shells, punctate brachiopods fragments, and foraminifera. Angular and subrounded micritic intraclasts, sometimes bioclastic wackestone intraclasts, and smaller rounded mud peloids formed by fragmentation of intraclasts are common non-skeletal constituents. Fine-sized subhedral or anhedral crystals of detrital quartz characterized by undulose extinction are also present. The compaction and pressure solution of allochems is evident along the irregular stylolitic contacts intersecting them. The non-stratified and coarse-grained lithofacies C do not reflect any cyclic pattern and evinces a complete absence of ammonite content.

The MJ-2 second-order Cycle

The MJ-2 Cycle (onset of the Niortense Chronozone – end of the Parkinsoni Chronozone) is almost entirely absent. In the northern flank of the volcanic mound, the MJ-2 Cycle has only been found related to the mm- or cm-thick infill of the hardground marking the previous MJ-1 Cycle boundary (CA-1, CA-2 and CA-17 stratigraphic logs). A mixed assemblage constituted by early Bajocian reelaborated

ammonoids along with late Bajocian (Niortense Chronozone) resedimented and reelaborated ones has been unearthed from the sedimentary fill of the hardground cavities. Fernández-López et al. (1985) reported *Oppelia* sp., *Strenoceras* sp., *Leptosphinctes* cf. *leptus* in their CAUDIÉL–XXIII stratigraphic log, and Cortés (2018) cited *Chondroceras* sp. (w), *Sphaeroceras* sp. (w), *Leptosphinctes* sp. (w), *Cleistosphinctes* sp. (w), *Caumontisphinctes* sp. (r/w) in CA–17 stratigraphic log.

In the southern flank of the volcanic mound (CA–65 stratigraphic log), a couple of beds, cm-thick each, crowned by hardgrounds have provided resedimented and reelaborated specimens with which the Niortense Chronozone has been identified again: *Oppelia* sp. (w), *Oecotraustes* sp. (w), *Stephanoceras* sp. (w), *Itinsaites* sp. (w), *Sphaeroceras* sp. (w), *Cadomites* sp. (r/w).

The MJ–3 second–order Cycle

The MJ–3 Cycle (onset of the Zigzag Chronozone – end of the Angulicostatum Chronozone) includes the Moscardón Formation and the lower half of the Domeño Formation. The Moscardón Formation is constituted by bioclastic packstone–grainstone limestones that display large-scale cross-bedding structures. The overlying Domeño Formation implies a marked vertical facies change into microfilament-dominated wackestone–packstone limestones. The Zigzag Chronozone shows a much greater thickness than other Bathonian chronozones. Fernández-López et al. (1985) and Fernández-López (1986) cited the presence of both late Bajocian (Niortense, Garantiana and Parkinsoni chronozones) reelaborated species (*Oecotraustes* sp., *Nodiferites* cf. *nodifer*, *Caumontisphinctes* sp., *Strenoceras* sp., *Garantiana* sp., *Hlawiceras* gr. *tetragonum*, *Lobosphinctes* sp.) and early Bathonian (Zigzag Chronozone) resedimented species (*Procerites* sp.) in the basal part of the Moscardón Formation of their CAUDIÉL–XXVI stratigraphic log. Cortés (2018) reported the retrieval of early Bathonian (Zigzag Chronozone) resedimented specimens (*Procerites* sp. and *Planisphinctes* sp.) coupled with late Bajocian (Garantiana and Parkinsoni chronozones) reelaborated specimens (*Paroecotraustes* sp. and *Parkinsonia* sp.) in the lower part of the Domeño Formation (CA–8 stratigraphic log).

On the other hand, the end of the MJ–3 Cycle is marked by a significant, traceable and widespread hardground located in the middle part of the Domeño Formation. About 0.50 m below this hardground, Fernández-López et al. (1985) still refer the presence of early Bathonian (Zigzag Chronozone) resedimented and reelaborated ammonoids: *Oxycerites* sp. (w), *Zeissoceras* cf. *primaevum* (w), *Alcidellus* cf. *costatus* (w), *Morphoceras* sp. (r) and *Procerites* sp. (r) from their CAUDIÉL–XXVI stratigraphic log.

It is only in CA–11 stratigraphic log and surrounding areas where the sea floor underwent small subsidence after the uppermost hardground was generated. The new and almost negligible accommodation was occupied by a 0.10 m-thick bed of limited lateral length and capped by an additional hardground. In this bed, *Cadomites* sp. (w), *Oxycerites* sp. (w), *Prohecticoceras* sp. (w), *Siemiradzka* sp. (w), *Nodiferites* sp. (w), and *Prevalia* sp. (w) could define the Retrocostatum Chronozone; however, the reelaborated taphonomic state of all the specimens raises doubts about this definition.

In summary, a possible Retrocostatum Chronozone, or any younger, is represented by rock bodies up to a maximum of 0.10 m thick, which contrast with the average thickness of 25 m of the Zigzag Chronozone succession. It has not been found any fossil record that allows an accurate identification of *Progracilis*, *Subcontractus*, *Bremeri*, *Retrocostatum*, and *Angulicostatum* chronozones.

The MJ–4 second–order Cycle

The MJ–4 Cycle (onset of the Bullatus Chronozone – end of the Lamberti Chronozone) comprises the upper half of the Domeño Formation and an unknown portion of the Arroyofrío Bed. The ammonite content has only enabled the determination of the Callovian age or, at most, the early Callovian, as evidenced by Fernández-López et al. (1985). It has been not possible to use the specimens found for chronozonal diagnosis.

Discussion

Nature and age of the volcanic phase

The explosive nature of submarine eruptions can be driven by the high concentrations of superheated magma volatiles, but also by the interactions between

the ambient seawater and incandescent magmatic rocks. Explosive eruptions tend to decrease as the depth increases. The hydrostatic pressure increases with depth and the explosive behavior decreases, since most of the volatile content remains confined inside the magma bodies. The gas pressure in molten magma bubbles needs to overcome the hydrostatic pressure to enable the explosive expansion to take place (Cas & Wright, 1987; Cas, 1992; White et al., 2003; Cas & Giordano, 2014). The great amounts of fragmental volcanoclastic products as against negligible amounts of lava in the Caudiel outcrop are consistent with an explosive volcanic activity in shallow submarine environments. This agrees with the sedimentological features observed on their host carbonate rocks. Lateral grading from lavas to largely reworked fine-grained epiclastic or volcano-sedimentary deposits constitutes the typical shifting described for marine stratovolcanoes, in which lava flows are associated with their central cores (Cas, 1992; Kralj, 2012). Consequently, this approach could be applied to the Caudiel volcano, and lava flows may be considered as an indicator of source-vents proximity (Fig. 7).

Once the eruptive activity ceased, the volcanic edifice should have been prone to summit and flank post-eruptive instability due to the action of the storm waves, currents and, occasionally, of fair-weather waves. Downdip epiclastic gravity flows must have happened frequently before cementation and lithification. They lead to the migration and expansion of the original boundaries, as well as to the formation of isolated volcanoclastic patches as detached portions of the mound. It becomes difficult to distinguish syn-eruptive gas-supported flow systems (primary subaqueous pyroclastic flow deposits) from the ones caused by syn-eruptive water-supported mass flows (primary debris flows or turbidite current deposits), even from those resulting of post-volcanic sedimentary reworking (secondary epiclastic deposits). However, it is evident that several calcareous beds lying on the lower part of both volcanic flanks were covered by lateral spreads of epiclastic spills, thus remaining, with the passage of time, as intervolcanic sedimentary beds (as can be seen in CA-12, CA-57 and CA-61 stratigraphic logs) (Figs. 3, 4, 7, 8). The volcanoclastic products that overlie these cm-thick sedimentary beds must

be considered, undoubtedly, as the outcome of post-volcanic sedimentary activity.

All the ammonoids collected from the intervolcanic sedimentary beds identify the Concavum Chronozone (Aalenian), but their reelaborated taphonomic state turns them into unsuitable indicators of age. Thus, the host beds that contain these ammonoids could have been deposited during the Concavum Chronozone or later.

In the far north of the outcrop (CA-1 stratigraphic log) (Figs. 3, 7), overlying a 0.60 m-thick layer of volcano-sedimentary deposits, a 0.50 m thick bed of bioclastic wackestone-packstone contains *Haplopleuroceras mundum* (r), *Eudmetoceras* sp. (w) and *Fontannesia* sp. (w). This assemblage could be indicating both the top of the Concavum Chronozone (late Aalenian) and the base of the Discites Chronozone (early Bajocian). Given that the uppermost pre-volcanic sediments are Aalenian (Concavum Chronozone) in age, the time of the volcanic event is constrained to the Aalenian-Bajocian boundary or, preferably, to the latest Aalenian (Cortés & Gómez, 2016; Cortés, 2018), since none of the typically indicative forms of the Discites Chronozone has made the first appearance yet. From this conclusion, it can be inferred that the deposition of carbonate layers interbedded around the pinching-out zones of both volcanic flanks took place shortly after the accumulation of volcanic matter. Later, the cementation of the volcanoclastic body may have occurred from the Propinquans Chronozone on, as no new beds hosted in volcanic flanks have been detected.

Reconstructing the volcanic mound and Middle Jurassic sediments

The ratio between length (about 3 km) and height (nearly 50 m) confers a gentle-slope mound morphology to the volcanic deposit. Obviously, not all the length of the mound corresponds to the flanks, but, still, even the length of the flank zones divided by the maximum height in the highest point of each flank does not provide too steep slopes. The average slope angle of the northern flank is circa 4 degrees, while the average angle of the southern flank is about 2.54 degrees.

The Arroyofrío Bed has been chosen in this work as the most representative reference line (datum) to

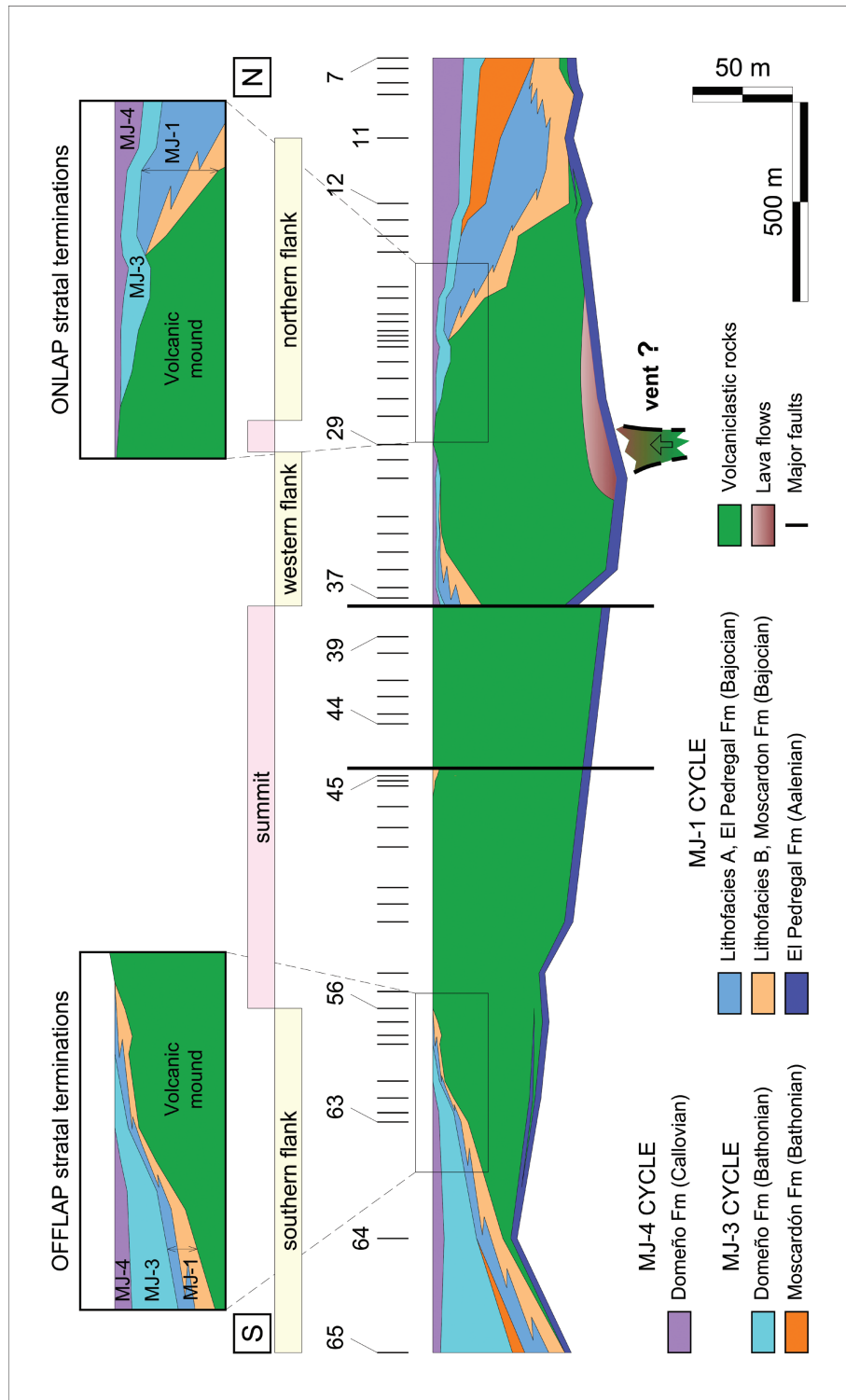


Figure 7.—Reconstruction of the entire volcanic mound and sediments of the MJ (Middle Jurassic) cycle across a N–S section. The north–central section has been interpreted as a western flank of the mound (see explanation in the text). Note the progressive onlap of younger sediments onto the north flank of the volcanic edifice, as well as the offlap stratal terminations onto the south flank.

be used as the starting point of the sketch (Fig. 7), by considering the following bases: 1) a volcanic mound summit is the area that is finally covered by the youngest stratigraphic unit of those draping the flanks, 2) the summit sectors might not necessarily correspond to the maximum height stretches of the mound, and 3) The Arroyofrío Bed is the stratigraphic unit that definitely overlies the last uncovered sectors of the mound. By locating the reference datum at the top of the mound instead of at the bottom, the differential subsidence and seabed instability conditions will be highlighted.

Based on the data set obtained from 65 stratigraphic logs, a two-dimensional reconstruction of the Middle Jurassic volcanic and sedimentary rocks has been modeled along a N–S cross-section (Cortés, 2018). Figure 7 shows the entire mound rebuilding and the two flank zones that can be observed: one to the north (CA–12 to CA–29 stratigraphic logs) (see also Figs. 3, 8A) and the other to the south (57 to 65 stratigraphic logs) (see also Figs. 4, 8B). Nevertheless, from CA–29 to CA–37 stratigraphic logs, a new flank area can also be seen, interpreted to be an apparent flank in relation to the N–S path. Along this stretch, the outcropping profile changes from N–S to NE–SW or even to ENE–WSW, so that what is really being observed is a western flank zone of the mound (Fig. 3).

The arrangement of carbonate sediments onlapping the volcanic mound over its north flank is not the same as over its south flank. Greater volcanic thicknesses in the north flank are covered by the Domeño Formation (Bathonian) or even the El Pedregal Formation (Bajocian), while smaller volcanic thicknesses in the south flank are directly overlain by the Arroyofrío Bed (Callovian–Oxfordian). As discussed below, this could be the result of downwarping and tilting movements of the floor once the release of the volcanic products concluded. If so, they should be considered as the major sedimentary controls.

Middle Jurassic tectonosedimentary evolution

MJ–1 Cycle

In well-expanded carbonate successions of the Iberian Basin, the MJ–1 Cycle began with El Pedregal Formation sediments resting on the basinal-scale

intra–Murchisonae unconformity which marked the lower boundary of this second-order MJ–1 Cycle (Fernández-López, 1997a,b; Fernández-López & Gómez, 2004; Gómez & Fernández-López, 2004a,b, 2006). In the Caudiel outcrop, however, the sedimentation began during the Bradfordensis Chronozone. No evidence of the post-unconformity Murchisonae Chronozone has been found, which enables the inference of regionally wider gaps in shallower and poor-expanded successions like this one.

Aalenian sediments (Bradfordensis and Concavum chronozones) represent successions deposited under low sedimentation rate conditions (stratigraphic condensation), containing mixed fossil assemblages (taphonomic condensation). However, they constitute, probably, expanded sediments (with no sedimentary condensation) deposited under high accumulation rates and separated by non-depositional or erosional gaps (Gómez & Fernández-López, 1994). Even so, Aalenian deposits can be found in the whole outcrop with non-substantial variations in thickness and, even, in sedimentary distinctive features. As previously stated, volcanic accumulation was emplaced around the Aalenian–Bajocian boundary, and it is only later (Bajocian) that non-uniform variations in both thickness and facies of the sedimentary infill are appreciated.

To begin with, a description of post-volcanic sediments on the north part of the volcanic mound will be made. Firstly, a significant hiatus was identified along which erosional and/or non-depositional steady conditions were placed on the depositional surface during the Discites and Laeviuscula chronozones (Fernández-López et al., 1985), probably over virtually the entire outcrop. This omission suggests a late Concavum–early Propinquans uplift (lasting about 400 ka, according to Ogg & Hinnov, 2012) that suppresses the accommodation space and precludes sedimentation. It was along this interval that the volcanic edifice was more likely to be eroded at the top and even to be emerged. In fact, lateral epiclastic landslides driven by the wave effect occurred at some point in the time interval between the end of the Concavum Chronozone and the onset of the Propinquans Chronozone. Nevertheless, as explained above, this must have happened relatively shortly after the volcanic accumulation.

On the other hand, lithofacies A, B, and C of post-volcanic Bajocian sediments exhibit similar

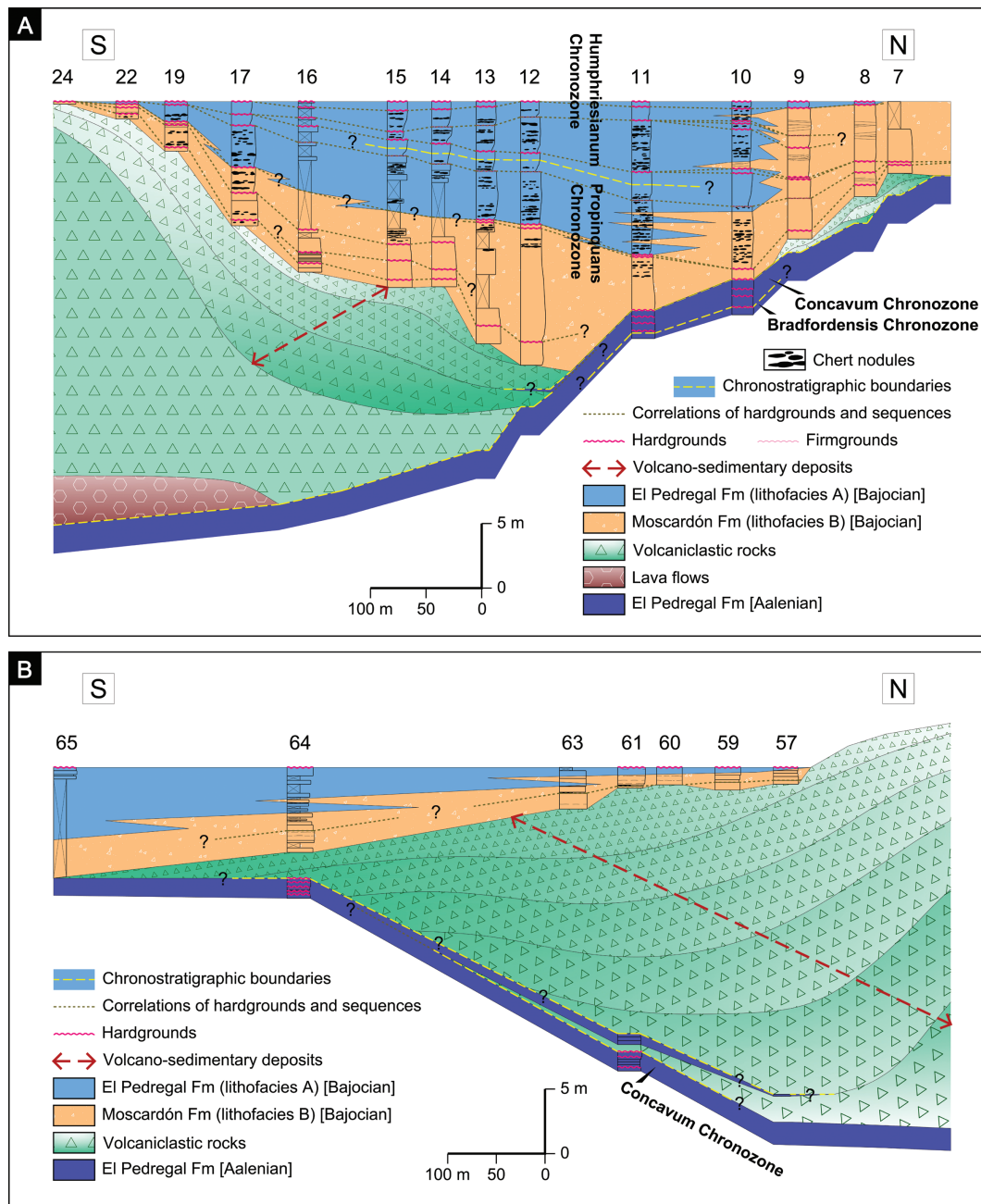


Figure 8.—2D depositional architecture reconstruction during the early Bajocian. **A**) Northern flank. **B**) Southern flank. Numbers (7 to 24 and 57 to 65) refer to stratigraphic logs numbers.

components, but they differ in whether intra-particle porosity has been infilled by micritic matrix or calcite cement, and in their distinctive sedimentary structures. All these features seem to point to variable energy conditions and distinct bathymetric locations on the platform. Lithofacies A (bioclastic wackestone-packstone limestones with chert

nodules) is interpreted to have been deposited in a relatively shallow open platform. The ammonite content in lithofacies A is probably restricted only to adult forms which could have reached these shallow areas as a result of the dispersion that affects the floating shells of dead specimens. Taphonomic-resedimented taxa have characterized the Propinquans

and Humphriesianum chronozones. Lithofacies B (massive wackestone to grainstone, mainly crinoidal limestones) is interpreted to be originated by gravity flow processes. The triggering mechanism for gravity flow deposits was probably the sweeping effect of waves and currents over the upper parts of the volcanic edifice (Fig. 9A). Sessile crinoids colonized the summit and flank environments of the mound, and, once they died, their remains were transported down

the slope and deposited as successive avalanche bodies at both the lower part and the base of the flanks (Gómez, 1979; Cortés & Gómez, 2016). The numerous internal erosional surfaces suggest multiple and successive events. Ammonoids are virtually absent in the coarse lithofacies B, though Fernández-López et al. (1985) were able to identify the Propinquans Chronozone at the base of a lithofacies B set, immediately above the Aalenian sediments and beyond the

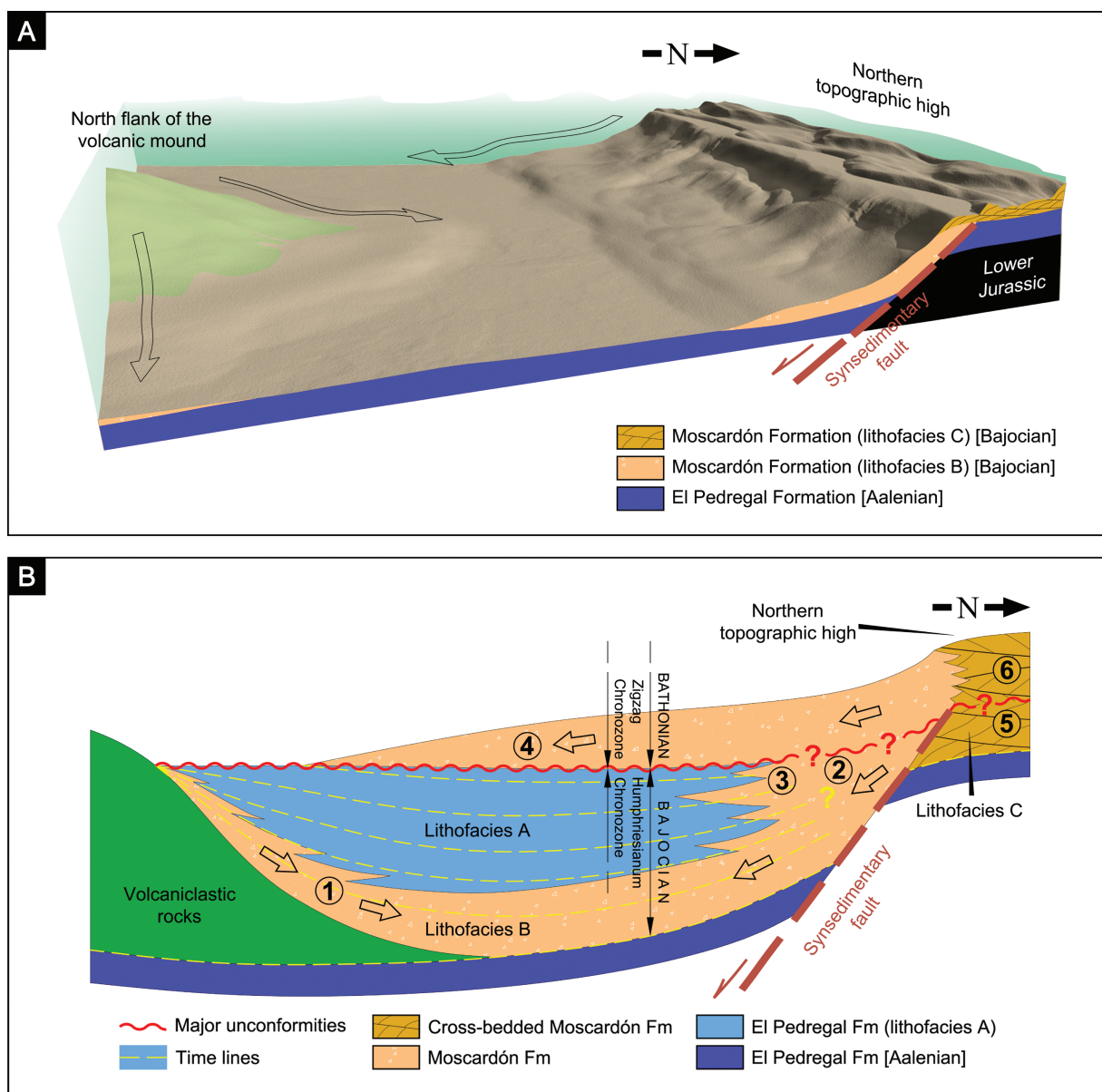


Figure 9.—Synsedimentary fault driving dynamic topography in the northern part of the Caudiel outcrop. **A**) 3D reconstruction during early Bajocian (Propinquans Chronozone) times (not to scale). **B**) 2D reconstruction of the early Bajocian and early Bathonian sedimentary filling (not to scale). See Figure 10 for legend of the numbers inside the circles.

point at which the volcanic mound is no longer present. Lithofacies C (bioclastic grainstone limestones), with high-energy features such as cross-stratification, is interpreted as the product of migrating shallow subtidal shoals (Fig. 9A). The lack of ammonites throughout the whole lithofacies C suggests inhospitable living conditions and/or unfavorable conditions for their preservation.

As stated above, the MJ-2 Cycle has not been recorded in the Caudiel outcrop. The sedimentation in the Bajocian time ceased abruptly towards the end of the Humphriesianum Chronozone. Since it is assumed that the position of the platform bottom had not fundamentally changed from the onset of the Niortense Chronozone until the end of the Parkinsoni Chronozone (length of time the MJ-2 Cycle) in the Caudiel outcrop, the top of the El Pedregal Formation, concurrent with the upper boundary of the MJ-1 Cycle, is assessed as the most appropriate surface to become the reference datum of this cycle for schematic representations. Figures 8A and 9B schematically illustrate the time-space distributions and relationships between lithofacies A, B, and C along a cross-section constructed through the northern flank of the volcanic mound. When the flat and uniform surfaces at the top are used, the tectonostratigraphic relationships of the units below can be evidenced by the observation of uneven bottoms, differential subsidence and variations in infilling thickness, despite the fact that the vertical scale has been strongly exaggerated. The thicknesses of Bajocian sediments vary quickly depending on the sector considered, suggesting an influence of the substrate movement on the thickness variation. It is obvious that the volcanic mound implied a significant relief on the sea bottom that reduced, if not precluded, the post-volcanic sedimentation. However, a flat-topped reconstruction reveals that the mound was not the only relief present during the Bajocian deposition. A topographic high of similar magnitude appears to be developed towards the northernmost part of the outcrop, so that the sedimentation fills the small basin-like space formed between the ramp that dips gently off the northern high and the north flank of the mound. Lithofacies B deposits extend throughout both slopes and the merging area, which is consistent with downdip gravitational deposition derived from the two areas of high topography.

As can be seen in Figures 8A and 9B, lithofacies B sediments usually are slightly older (base of the Propinquans Chronozone) than those of lithofacies A (top of the Propinquans Chronozone-top of the Humphriesianum Chronozone) except in the northern basin margin. At this site, the contact between a relatively lower-energy lithofacies A and a higher-energy lithofacies B takes place through a lateral and jagged facies change within a section of comparable age. Therefore, it seems that lithofacies B sediments coming from the volcanic mound are limited to the areas near the flank and the foot of the slope, while lithofacies B sediments that originate from the northern topographic high are far more laterally expansive.

High-energy lithofacies C environments are restricted to the top of the northern structural high, constituting the source area for gravity-induced coarse-grained lithofacies B on the northern slope. Storm waves and currents are interpreted to be the dominant triggering mechanism by which remobilized parts of banks and shoals overstep the margin of the structural high, shedding off and tumbling down the slope under the influence of gravity. To be more precise, the cross-bedded bioclastic grainstones lying on the Aalenian substrate to the north of the Caudiel outcrop do not undergo vertical facies changes along the total thickness of the section until the base of the next overlying Domeño Formation. Due to the absence of ammonites, the boundary Bajocian-Bathonian cannot be traced with certainty within the stratigraphic interval. However, an undetermined lower portion of the cross-bedded bioclastic grainstones must be Bajocian in age to constitute the device formed by shoal facies located at the top of the topographic high and by gravitational sliding facies on the slope (Figs. 9B, 10). Therefore, the gravitational sliding deposits, which are coeval with the well-dated lithofacies A sediments form the Bajocian lithofacies B, and the lower portion of the cross-bedded bioclastic grainstones, presumably Bajocian in age, composes the lithofacies C (Figs. 9B, 10).

The concurrence of nearly 50 m-thick non-emerged volcanic deposits compared to a very reduced marine depth, represented by the bioclastic shoal complex to the north, is better explained when the subsidence affecting the volcanic mound is

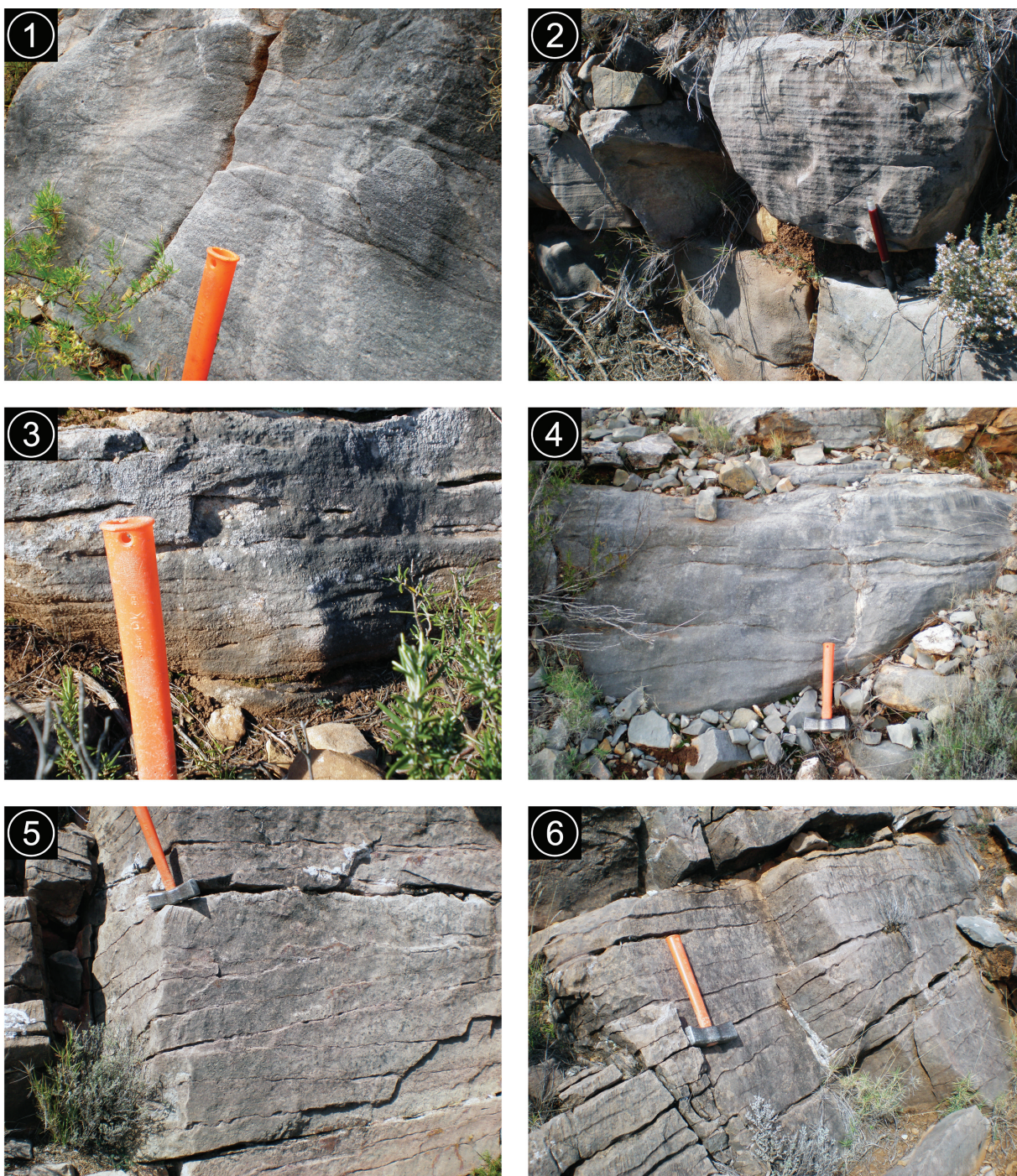


Figure 10.—Field views showing the strong similarity in the external appearance and sedimentary structures between the sediments of the Moscardón Formation regardless their age. **1:** Bajocian lithofacies B (Moscardón Fm) in CA–14 stratigraphic log. **2:** Bajocian lithofacies B (Moscardón Fm) in CA–8 stratigraphic log. **3:** Bajocian lithofacies B (Moscardón Fm) in CA–9 stratigraphic log. **4:** Bathonian (Moscardón Fm) in CA–11 stratigraphic log. **5:** Bajocian(?) lithofacies C (Moscardón Fm) in CA–4 stratigraphic log. **6:** Bathonian(?) cross-bedded crinoidal calcarenites (Moscardón Fm) in CA–4 stratigraphic log. Hammer and pencil for scale are respectively 27 and 14 cm length.

considered. Such configuration requires the existence of two domains which had different subsidence rates and were controlled by an inferred syndepositionary fault. The hanging wall block comprising the volcanic mound moves downward relative to the northern structural high represented by the footwall block.

On the other hand, the lateral distribution of unconformities (firm- and hardgrounds) between CA-7 and CA-24 stratigraphic logs (Fig. 8A) is also significant. The shallowing-upward sequences formed by lithofacies A, as well as the non-cyclic massive intervals of lithofacies B, are bounded by firmgrounds or hardgrounds. In Figure 8A, lateral correlations between firmgrounds and hardgrounds have been drawn within the Bajocian sedimentary succession on the northern flank of the volcanic mound. As can be seen, the lines of correlation tend to converge and overlap until their pinching out on the updip flank of the mound. The form described by the correlation lines, converging upwards to the highs and flexing downwards to the trough, suggests that the bottom subsided favored by syndepositionary faulting. This subsidence resulted in the creation of accommodation that was progressively and simultaneously filled up with sliding sediments coming from the highs. The confluence of the correlation lines towards the northern high reveals how the bedding planes tend to be slightly deformed (normal drag folding near the fault) resulting in a gentle hanging wall syncline (Fig. 8A). The dip of the slopes (flank of the mound and wall of the structural high) is smooth; nevertheless, gravity-flow sediments do not seem to need high slope gradients to slide. Submarine slides happen on modern slopes of less than 4° (Shanmugam, 2016). In the slopes that connect the shallow-water carbonate platforms of the Bahamas with the deeper water areas, Eberli (1988) reported that carbonate turbidites start to accumulate on slopes with declivities of less than 3°. In the margin of the Upper Devonian Ancient Wall carbonate complex of Alberta (Canada), Cook & Mullins (1983) described a 1 m-thick bed that was interpreted as a probable grain-flow deposit. This bed may have been initiated on slopes of 5 to 10°, but after about 1 km it moved across gradients of probably less than 2°.

Later (during the Humphriesianum Chronozone), lithofacies A arranged into shallowing-upward sequences in the central part of the basin-like space,

away from the mound influence. Meanwhile, the northern mechanism continued to operate and to provide lithofacies B sediments around the syndepositionary fault.

In the southern part of the volcanic mound, substantial thickness reductions of the post-volcanic sediments belonging to the MJ-1 Cycle can be observed as compared to thicknesses measured on the north flank (Figs. 7, 8B). The thickness of the volcanic rocks is also smaller in this southern flank. Post-volcanic sediments of the MJ-1 Cycle have not been able to be accurately dated as no ammonoids have been found. They are assigned to the early Bajocian because the sedimentary facies are similar to those of the north flank, especially to lithofacies B, but basically because they are stratigraphically positioned above the well-dated Aalenian succession and below several thin beds that are late Bajocian (Niortense Chronozone) in age (CA-65 stratigraphic log). Lithofacies B sediments deposited on the south volcanic flank must come from the sweeping of dead crinoid remains on the summit and slope, as in the case of the north flank. Central parts corresponding to the summit and upslope areas of the volcanic mound have remained non-covered by sediments at the end of MJ-1 Cycle, to be covered later by Bathonian and Callovian strata.

The highest rates of subsidence and the greatest sedimentary thickness occurred around the north flank of the volcanic mound, while lower rates of subsidence appear to have led simultaneously to smaller sedimentary accumulations on the south flank of the volcanic mound. All these features are compatible with a half-graben-like depression structure, where the downthrown block is north-dipping against the surface of the syndepositionary fault. A pivoting zone has been tentatively located towards the middle part of the volcanic mound to account for the rotating motion of the down-dropped ground, probably favored by not a planar, but rather a curved, fault plane (Fig. 11A).

In the southernmost point of the platform under the volcanic mound, there must exist a new hinge zone that worked against the northward dipping in order not only to prevent the emersion of the most distal parts of the southern seafloor, but also to implement the southward creation of accommodation (Fig. 11A).

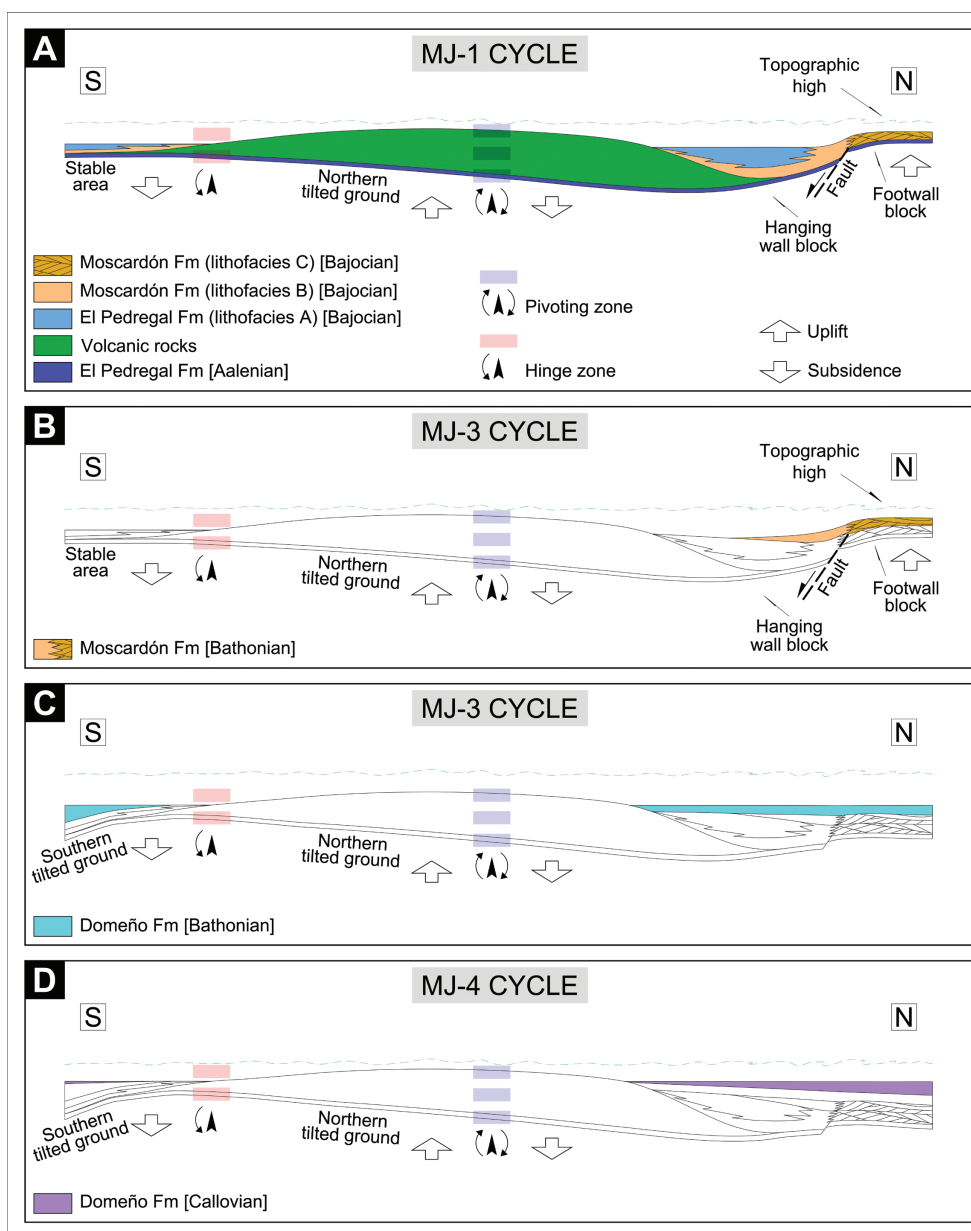


Figure 11.—Synthetic sketch (not to scale) showing the Middle Jurassic tectonosedimentary evolution during MJ-1 Cycle (A), MJ-3 Cycle (B, C) and MJ-4 Cycle. See text for explanation.

MJ-2 Cycle

There is virtually no sedimentary record throughout the whole MJ-2 second-order Cycle in the Caudiel outcrop. Two alternative approaches may be envisaged concerning the null or minimum accommodation that occurred at the time when this sedimentary cycle developed: (1) if tectonism was the only mechanism

for accommodation generation on a basinal scale, then it can be claimed that no subsidence took place in the Caudiel outcrop from the onset of the Niortense Chronozone to the end of the Parkinsoni Chronozone, (2) if the creation of accommodation was mainly eustatic in origin, the Caudiel outcrop had to undergo uplift able to compensate the global accommodation that was created along this time interval.

MJ-3 Cycle

The MJ-3 Cycle is characterized by the alternation of subsidence–uplift. After an extended sedimentary gap (MJ-2 Cycle), the sedimentation resumed during the early Bathonian Zigzag Chronozone with coarse–grained lithofacies of the Moscardón Formation. The shoals field/gravitational flows system induced by the half–graben activity remained active at the beginning of the MJ-3 Cycle (Bathonian Zigzag Chronozone) just like in the early Bajocian (Propinquans and Humphriesianum chronozones). This happened to such an extent that Bajocian lithofacies B sediments (MJ-1 Cycle) are indistinguishable from the overlying limestones of the Bathonian Moscardón Formation (MJ-3 Cycle, CA-7 to CA-10 stratigraphic logs). Similarly, the Bajocian lithofacies C (MJ-1 Cycle) and the beds of the overlying Bathonian Moscardón Formation (MJ-3 Cycle) cannot be distinguished on the northern topographic high (CA-4 to CA-6 stratigraphic logs) (Fig. 10). It is therefore likely to include Bajocian lithofacies B and C within the Moscardón Formation. Its lower boundary is dated, consequently, as Propinquans Chronozone in the northern part of the Caudiel outcrop. It is unclear whether the still lifted and uncovered parts of the volcanic mound could provide bioclastic input, but it is a fact that sediments of the Bathonian Moscardón Formation pinch out onto El Pedregal Formation beds instead of overlying the volcanic slope (Figs. 9B, 11B).

In the southernmost point studied, 3 m of sediments belonging to the Moscardón Formation (above the well–dated beds as late Bajocian in CA-65 stratigraphic log) have been observed, but their age is uncertain, ranging from late Bajocian to early Bathonian. In any case, as the northward tilted ground persisted to favor a renewed shoals/slides system, the hinge zone of the south flank had also been activated both to prevent the most distal parts of the southern seafloor from being subaerially exposed, and to place the platform ground around the submarine erosional–depositional boundary (Fig. 11B).

Later, still during the Zigzag Chronozone, the high–energy and coarse–grained sediments of the Moscardón Formation were replaced abruptly by finer limestones belonging to the Domeño Formation.

This indicates a rapid and significant deepening of the depositional environment. The northern structural high sank and ceased to be an important supply source paleogeographic element. The half–graben and its related synsedimentary fault will no longer act.

In the northern flank, the Domeño Formation (MJ-3 Cycle) has been found now to be much more expanded than the Moscardón Formation, since it overlies practically the entire northern volcanic flank that had remained uncovered until that time. In addition, the infilling of the accommodation space seems to be indicative of a homogenization in subsidence patterns (Figs. 7, 11C).

However, in the southern flank, the Domeño Formation shows less expansion as it pinches out onto the Bajocian Moscardón Formation and does not overlie the volcanic rocks. This points to lower rates of subsidence than in the northern flank, even to a slight uplifting. Nevertheless, increasing thickness can be observed farther southward from the southern hinge zone (Figs. 7, 11C).

The upper part of the Moscardón and the lower part of the Domeño Formation have been deposited during early Bathonian Zigzag Chronozone times with almost no record of subsequent Bathonian chronozones. A generalized uplifting seems to have taken place once again, competing with global or regional creation of accommodation throughout the middle and late Bathonian.

MJ-4 Cycle

It has not been possible to determine an accurate chronostratigraphy of the Callovian (Domeño Formation, MJ-4 Cycle) in the Caudiel outcrop. However, Fernández–López et al. (1985) assigned an early Callovian age to the upper part of the Domeño Formation, below the Arroyofrío Bed, in their CAUDIÉL–VI and CAUDIÉL–XXVI stratigraphic logs. Thus, it is very likely that tectonic patterns operated in a similar way to that of the previous MJ-3 Cycle; that is, an uplift following the initial subsidence. In any case, a homogeneous subsidence pattern can be identified by comparing the thicknesses of the Callovian Domeño Formation observed in both flanks of the volcanic mound. However, the greater thickness on the northern flank could be linked to a possible tilting northward of the

ground (Fig. 11D), perhaps related to some normal fault located away of the area studied.

Stratal terminations onto pre-existing volcanic relief as evidence of synsedimentary tectonism

MJ-1, MJ-2, MJ-3, and MJ-4 second-order cycles, which are correlated on a regional scale (Iberian Basin), are strongly distorted in the Caudiel outcrop. Superimposed to any eustatic or tectonoeustatic signal, there is a local, recurring and seemingly random tectonic pattern consisting of subsidence followed by uplifting or, conversely, uplifting followed by subsidence within each cycle. The successive post-volcanic lithostratigraphic units overstep each other to onlap the volcanic north flank, with the exception of the Bathonian Moscardón Formation (MJ-3 Cycle), which overlies only a part of the El Pedregal Formation (MJ-1 Cycle) (Fig. 7). However, an offlap stratal termination onto the south volcanic flank can be observed (Fig. 7), so that each younger unit leaves a non-covered portion of the previous older unit on which it lies (following the descriptions of stratal geometries by Catuneanu, 2006, 2019). From a purely eustatic perspective, coeval onlap-offlap stacking geometries are incompatible, since the onlap is considered to form only during stages of base level rise, while offlap stratigraphic terminations are the product of base level fall and, hence, diagnostic for forced regressions (Catuneanu, 2006, 2019).

The onlap and offlap stratal terminations that developed simultaneously on each volcanic flank are evidence of local tectonic control. The subsidence and uplifting effects driven by platform tilting, usually subsidence towards the north flank and uplifting towards the south flank of the mound, could successfully explain this simultaneity. The northward rotating tilting of the hanging wall block around the pivoting zone seems to be an inherent consequence of the half-graben activity itself. Opposite southward tilt movements are needed around a southern hinge to prevent the emersion and favor the offlapping stacking pattern and the expansion of the sedimentation area to the south.

Poor outcropping conditions have not allowed the accurate in situ recognition of the active synsedimentary dip-slip fault track, which is the one that defines

the half-graben-like structure. It is unclear whether the fault keeps the general trace of the Caudiel Fault Zone or, on the contrary, it follows an oblique direction. Be that as it may, it probably constitutes an integral part of the fault zone itself.

Conclusions

1) New studies focused on the stratigraphy and tectonosedimentary evolution of the volcano-bearing Middle Jurassic marine carbonate sediments in the Caudiel region have revealed local tectonic activity consisting of repetitive vertical displacements of the ground. Tectonism was able to obliterate long-term eustatic or tectonoeustatic signals and it significantly precluded sediment deposition intermittently. Long time periods of no deposition have been identified with adequate biostratigraphic control within the MJ-1 Cycle (affecting the Discites and Laeviuscula chronozones), along the entire MJ-2 Cycle, within the MJ-3 Cycle (spanning almost the whole Bathonian, except for the Zigzag Chronozone), and, possibly, in some parts of the MJ-4 Cycle. Once the uplift phases ceased, sedimentation resumed during the Propinquans and Humphriesianum Bajocian chronozones, the Zigzag Bathonian Chronozone, and probably during the early Callovian. Therefore, Middle Jurassic deposition took place only over a few chronozones.

2) A dynamic topography keeping pace with sedimentation can be inferred from the study of the sedimentary infilling, especially throughout the Bajocian time. An abrupt northward lateral shift from fine-grained lithofacies to coarse-grained and cross-bedded lithofacies reflects the presence of a topographic high that is here characterized for the first time. Lithofacies B, coming from the source-area uplifted, is stacked as slope-base fans between the downwarping area, where the fine-grained lithofacies A was deposited, and the topographic high, dominated by bioclastic shoal fields (lithofacies C). Thus, it can be concluded that the platform was affected by tectonic activity giving rise to the development of at least one identified half-graben-like structure which involved the previously released volcanic rocks. The entire volcanic mound was located over the hanging wall block, while the topographic high is developed on the footwall block northward the studied area.

The hanging wall block, in turn, underwent N–dipping, so that the northern volcanic flank subsided at the same time as the southern volcanic flank uplifted. The onlap stratal terminations of Bajocian, Bathonian and Callovian sediments onto the north volcanic flank, along with the offlap geometry of coeval sediments onto the south volcanic flank, provide evidence for the effect of the synsedimentary ground tilting.

Despite the observed differential subsidence, the volcanic mound represented a significant relief over the sea floor, comparable in magnitude to the northern topographic high, at all times. The accumulated volcanic masses reduced the available accommodation, and their colonization by crinoids occurred, contributing to drastic changes seen in the expected Bajocian microfilaments–bearing lithofacies, just as previously argued by Gómez (1979).

ACKNOWLEDGEMENTS

Thanks to Professors Sixto Rafael Fernández–López and Soledad Ureta Gil (Universidad Complutense de Madrid) for their taxonomic and taphonomic determinations of ammonoid specimens. The author greatly appreciated the review comments and suggestions from Professor Juan José Gómez Fernández (Universidad Complutense de Madrid) before manuscript submission. I am very grateful to Vice–Chair of International Subcommission on Jurassic Stratigraphy, Prof. Emanuela Mattioli, and to Dr. Luis Alcalá Martínez (Fundación Dinópolis, Teruel) for their valuable comments and contributions about formal chronostratigraphic nomenclature. Constructive suggestions and comments from the editor José María Cebría and two reviewers, Prof. Alberto Pérez López (Universidad de Granada) and Prof. Marcos Aurell Cardona (Universidad de Zaragoza), helped to improve the original manuscript. The author also acknowledges Raquel Fuertes Ortega, Msc. for the language proofreading of the manuscript.

References

- Abril, J.; García, F.; González, F.; Iglesias, M.; Ortí, F. & Rubio, J. (1975). Hoja geológica núm. 638 (Alpuente). Mapa Geológico de España E. 1:50 000. Segunda serie. IGME, Madrid.
- Abril, J.; Apalategui, O.; Ferreiro, E.; García, F.; González, F.; Hernández, E.; Lago, E.; Ortí, F.; Pliego, D.V.; Quintero, I. & Rubio, J. (1978). Hoja geológica núm. 613 (Camarena de la Sierra). Mapa Geológico de España E. 1:50 000. Segunda serie. IGME, Madrid.
- Adrover, R.; Aguilar, M.J.; Alberdi, M.T.; Aragonés, E.; Aznar, J.M.; Comas, M.J.; Gabaldón, V.; Giner, J.; Godoy, A.; Goy, A.; Gutiérrez, M.; Leal, M.C.; Moissenet, E.; Olivé, A.; Portero, J.M.; Ramírez, J.I. & Ramírez del Pozo, J. (1983). Hoja geológica núm. 590 (La Puebla de Valverde). Mapa Geológico de España E. 1:50 000. Segunda serie. IGME, Madrid.
- Aurell, M.; Robles, S.; Bádenas, B.; Rosales, I.; Quesada, S.; Meléndez, G. & García–Ramos, J.C. (2003). Transgressive–regressive cycles and Jurassic palaeogeography of northeast Iberia. *Sedimentary Geology*, 162(3–4): 239–271. [https://doi.org/10.1016/S0037-0738\(03\)00154-4](https://doi.org/10.1016/S0037-0738(03)00154-4)
- Callomon, J.H. (2003). The Middle Jurassic of western and northern Europe: its subdivisions, geochronology and correlations. *Geological Survey of Denmark and Greenland Bulletin*, 1: 61–73.
- Campos, C.; González, F.; Goy, A.; Lazuen, J.; Martín, P. & Ortí, F. (1977). Hoja geológica núm. 639 (Jérica). Mapa Geológico de España E. 1:50 000. Segunda serie. IGME, Madrid.
- Cas, R.A.F. & Giordano, G. (2014). Submarine volcanism: a review of the constraints, processes and products, and relevance to the Cabo de Gata volcanic succession. *Italian Journal of Geosciences*, 133(3): 362–377. <https://doi.org/10.3301/IJG.2014.46>
- Cas, R.A.F. & Wright, J.V. (1987). Volcanic successions. Modern and ancient. Chapman and Hall, London, 528 pp. <https://doi.org/10.1007/978-94-009-3167-1>
- Cas, R.A.F. (1992). Submarine volcanism: Eruption styles, products, and relevance to understanding the host–rock successions to volcanic–hosted massive sulfide deposits. *Economic Geology*, 87(3): 511–541. <https://doi.org/10.2113/gsecongeo.87.3.511>
- Catuneanu, O. (2006). Principles of sequence stratigraphy. Elsevier, Amsterdam, 375 pp.
- Catuneanu, O. (2019). Model–independent sequence stratigraphy. *Earth–Science Reviews*, 188: 312–388. <https://doi.org/10.1016/j.earscirev.2018.09.017>
- Cook, H.E. & Mullins, H.T. (1983). Basin margin environment. In: Carbonate depositional environments (Scholle, P.A.; Bebout, D.G. & Moore, C.H., Eds.), The American Association of Petroleum Geologists, Tulsa. *Memoir* 33: 540–617.
- Cortés, J.E. (2018). La arquitectura deposicional de los carbonatos del Jurásico Inferior y Medio relacionados con los materiales volcánicos del sureste de la Cordillera Ibérica. Tesis doctoral, Universidad Complutense de Madrid, 1272 pp.
- Cortés, J.E. & Gómez, J.J. (2016). Middle Jurassic volcanism in a magmatic–rich passive margin linked to the Caudiel Fault Zone (Iberian Range, East of Spain): biostratigraphical dating. *Journal of Iberian Geology*, 42(3): 335–354. <https://doi.org/10.5209/JIGE.54667>
- Eberli, G.P. (1988). Physical properties of carbonate turbidite sequences surrounding the Bahamas–Implications for slope stability and fluid movements. In: Proceedings of the ocean drilling program, scientific results (Rose, W.D. & Stewart, S.K., Eds.), Ocean Drilling Program 101, Texas, 305–314. <https://doi.org/10.2973/odp.proc.sr.101.150.1988>

- Fernández-López, S. (1984a). Nuevas perspectivas de la tafonomía evolutiva: Tafosistemas y asociaciones conservadas. *Estudios geológicos*, 40(3-4): 215-224. <https://doi.org/10.3989/egeol.84403-4662>
- Fernández-López, S. (1984b). Criterios elementales de reelaboración tafonómica en ammonites de la Cordillera Ibérica. *Acta Geológica Hispánica*, 19(2): 105-116.
- Fernández-López, S.R. (1985). El Bajociense en la Cordillera Ibérica. I.- Taxonomía y Sistemática (Ammonoidea). II.- Bioestratigrafía. III.- Atlas. Tesis doctoral, Universidad Complutense de Madrid, 850 pp.
- Fernández-López, S. (1986). Sucesiones paleobiológicas y sucesiones registráticas (nuevos conceptos paleontológicos). *Revista Española de Paleontología*, 1(1): 29-45.
- Fernández-López, S. (1997a). Ammonites, ciclos tafonómicos y ciclos estratigráficos en plataformas epicontinentales carbonáticas. *Revista Española de Paleontología*, 12(2): 151-174.
- Fernández-López, S. (1997b). Ammonites, taphonomic cycles and stratigraphic cycles in carbonate epicontinental platforms. *Cuadernos de Geología Ibérica*, 23: 95-136.
- Fernández-López, S. & Gómez, J.J. (1990). Evolution tectono-sédimentaire et genèse des associations d'ammonites dans le secteur central du Bassin Ibérique (Espagne) pendant l'Aalénien. *Cahiers de l'Université Catholique de Lyon, Série Scientifique*, 4: 39-52.
- Fernández-López, S. & Gómez, J.J. (2004). The Middle Jurassic eastern margin of the Iberian platform system (eastern Spain). *Palaeogeography and bi-dispersal routes of ammonoids. Rivista Italiana di Paleontologia e Stratigrafia*, 110(1): 151-162. <https://doi.org/10.13130/2039-4942/6281>
- Fernández-López, S. & Mouterde, R. (1994). L'Horizon à Gervillii (Bajocien inférieur) de Tendron (Cher, France). Taphonomie et populations d'ammonites. *Proceedings 3rd International Meeting on Aalenian and Bajocian Stratigraphy. Miscellanea del Servizio Geologico Nazionale*, 5: 117-159.
- Fernández-López, S.; Gómez, J.J. & Goy, A. (1985). Sédimentologie des carbonates développés sur un "monticule" de matériaux volcaniques. In: *Le Jurassique des Ibérides Orientales (Espagne) (Canerot, J. & Goy, A., Eds.)*, Strata, serie 2: mémoires, vol. 2: 101-115.
- García-Frank, A. (2006). Evolución biosedimentaria y secuencial del Jurásico Medio inferior en la Cuenca Ibérica (Sector NO). Tesis doctoral, Universidad Complutense de Madrid, 529 pp.
- García-Frank, A.; Ureta, S. & Mas, R. (2006). Tectonically active Aalenian in the northwestern Iberian Basin (Spain). 7th International Congress on the Jurassic System. Poland-Kraków, September 6-18. Abstract book, *Volumina Jurassica*, IV: 42.
- García-Frank, A.; Ureta, S. & Mas, R. (2008). Aalenian pulses of tectonic activity in the Iberian Basin, Spain. *Sedimentary Geology*, 209(1-4): 15-35. <https://doi.org/10.1016/j.sedgeo.2008.06.004>
- Gautier, F. (1974). Hoja geológica núm. 614 (Manzanera). Mapa Geológico de España E. 1:50 000. Segunda serie. IGME, Madrid.
- Gómez, J.J. (1979). El Jurásico en facies carbonatadas del sector levantino de la Cordillera Ibérica. *Seminarios de Estratigrafía. Serie Monografías*, núm. 4. Universidad Complutense-Consejo Superior de Investigaciones Científicas, Madrid, 683 pp.
- Gómez, J.J. & Fernández-López, S. (1994). Condensation processes in shallow platforms. *Sedimentary Geology*, 92(3-4): 147-159. [https://doi.org/10.1016/0037-0738\(94\)90103-1](https://doi.org/10.1016/0037-0738(94)90103-1)
- Gómez, J.J. & Fernández-López, S. (2004a). Jurásico Medio. In: *Geología de España (Vera, J.A., Ed.)*, SGE-IGME, Madrid, 500-503.
- Gómez, J.J. & Fernández-López, S. (2004b). Las unidades litoestratigráficas del Jurásico Medio de la Cordillera Ibérica. *Geogaceta*, 35: 91-94.
- Gómez, J.J. & Fernández-López, S. (2006). The Iberian Middle Jurassic carbonate-platform system: Synthesis of the palaeogeographic elements of its eastern margin (Spain). *Palaeogeography, Palaeoclimatology, Palaeoecology*, 236(3-4): 190-205. <https://doi.org/10.1016/j.palaeo.2005.11.008>
- Gómez, J.J. & Goy, A. (1977). Estudio de las facies relacionadas con un montículo de origen volcánico en el Jurásico Medio de Caudiel (Castellón). *Abstracts VIII Congreso Nacional de Sedimentología*, Oviedo-León.
- Gómez, J.J. & Goy, A. (1979). Las unidades litoestratigráficas del Jurásico medio y superior, en facies carbonatadas del Sector Levantino de la Cordillera Ibérica. *Estudios Geológicos*, 35(1-2): 569-598.
- Gómez, J.J.; Aguado, R.; Azerêdo, A.C.; Cortés, J.E.; Duarte, L.V.; O'Dogherty, L.; Bordalo da Rocha, R. and Sandoval, J. (2019). 4. The Late Triassic-Middle Jurassic Passive Margin Stage. In: *The Geology of Iberia: A Geodynamic Approach. Vol. 3: The Alpine Cycle (Quesada, C. and Oliveira, J.T., Eds.)*, Springer, Switzerland, 113-167. <https://doi.org/10.1007/978-3-030-11295-0>
- Kralj, P. (2012). Facies architecture of the Upper Oligocene submarine Smrekovec stratovolcano, Northern Slovenia. *Journal of Volcanology and Geothermal Research*, 247-248: 122-138. <https://doi.org/10.1016/j.jvolgeores.2012.07.016>
- Lazuen, J. & Roldán, R. (1977). Hoja geológica núm. 667 (Villar del Arzobispo). Mapa Geológico de España E. 1:50 000. Segunda serie. IGME, Madrid.
- McCann, T. & Saintot, A. (2003). Tracing tectonic deformation using the sedimentary record: an overview.

- In: Tracing tectonic deformation using the sedimentary record (McCann, T. & Saintot, A., Eds.), Geological Society, London. Special Publication 208: 1–28. <https://doi.org/10.1144/gsl.sp.2003.208.01.01>
- Ogg, J.G. & Hinnov, L.A. (2012). Jurassic. In: The Geological Time Scale (Grandstein, F.M.; Ogg, J.G.; Schmitz, M.D. & Ogg, G.M., Eds.), Elsevier B.V., Amsterdam, 731–791. <https://doi.org/10.1016/B978-0-444-59425-9.00026-3>
- Ortí, F. & Sanfeliu, T. (1971). Estudio del vulcanismo jurásico de Caudiel (Castellón) en relación con procesos de lateritización, condensación y silicificación de la serie calcárea. Instituto de Investigaciones Geológicas de la Diputación Provincial. Barcelona, vol. XXVI: 21–34.
- Ortí, F. & Vaquer, R. (1980). Volcanismo jurásico del sector valenciano de la Cordillera Ibérica. Distribución y trama estructural. *Acta Geológica Hispánica*, 15(5): 127–130.
- Osete, M.L.; Gómez, J.J.; Pavón-Carrasco, F.J.; Villalain, J.J.; Palencia-Ortas, A.; Ruiz-Martínez, V.C. & Heller, F. (2011). The evolution of Iberia during the Jurassic from palaeomagnetic data. *Tectonophysics*, 502(1–2): 105–120. <https://doi.org/10.1016/j.tecto.2010.05.025>.
- Page, K. N. (2003). The Lower Jurassic of Europe: its subdivision and correlation. *Geological Survey of Denmark and Greenland Bulletin*, 1: 23–59.
- Santisteban, C. De (2016). La fracturación de la rampa carbonática del tránsito Jurásico Inferior a Medio y volcanismo asociado en el sector de La Salada (Sistema Ibérico, Teruel). *Geogaceta*, 60, 3–6.
- Santisteban, C. De (2018). El vulcanismo de La Concòrdia (Lliria, Valencia) y las discontinuidades adyacentes al límite Jurásico Inferior–Jurásico Medio, en el sector Suroriental del Surco Ibérico. *Geogaceta*, 63, 23–26.
- Schettino, A. & Turco, E. (2011). Tectonic history of the western Tethys since the Late Triassic. *Geological Society of America Bulletin*, 123(1–2): 89–105. <https://doi.org/10.1130/B30064.1>
- Shanmugam, G. (2016). Submarine fans: A critical retrospective (1950–2015). *Journal of Palaeogeography*, 5(2): 110–184. <https://doi.org/10.1016/j.jop.2015.08.011>
- Stampfli, G.M. & Borel, G.D. (2002). A plate tectonic model for the Paleozoic and Mesozoic constrained by dynamic plate boundaries and restored synthetic ocean isochrons. *Earth and Planetary Science Letters*, 196(1–2): 17–33. [https://doi.org/10.1016/S0012-821X\(01\)00588-X](https://doi.org/10.1016/S0012-821X(01)00588-X)
- Stampfli, G.M. & Borel, G.D. (2004). The TRANSMED transects in space and time: constraints on the paleotectonic evolution of the Mediterranean domain. In: The TRANSMED Atlas. The Mediterranean Region from Crust to Mantle (Cavazza, W.; Roure, F.M.; Spakman, W.; Stampfli, G.M. & Ziegler, P.A., Eds.), Springer, Berlin, Heidelberg, 53–80). https://doi.org/10.1007/978-3-642-18919-7_3
- Stampfli, G.M. & Hochard, C. (2009). Plate tectonics of the Alpine realm. In: Ancient orogens and modern analogues (Murphy, J.B.; Keppie, J.D. & Hynes, A.J., Eds.), Geological Society, London. Special Publication 327: 89–111. <https://doi.org/10.1144/SP327.6>
- Stampfli, G.M.; Borel, G.D.; Marchant, R. & Mosar, J. (2002). Western Alps geological constraints on western Tethyan reconstructions. In: Reconstruction of the evolution of the Alpine–Himalayan Orogen (Rosenbaum, G. & Lister, G.S., Eds.), *Journal of the Virtual Explorer*, 8: 75–104. <https://doi.org/10.3809/jvirtex.2002.00057>
- Vera, J.A.; Molina, J.M.; Montero, P. & Bea, F. (1997). Jurassic guyots on the Southern Iberian Continental Margin: a model of isolated carbonate platforms on volcanic submarine edifices. *Terra Nova*, 9(4): 163–166. <https://doi.org/10.1046/j.1365-3121.1997.d01-22.x>
- White, J.D.L.; Smellie, J.L. & Clague, D.A. (2003). Introduction: A deductive outline and tropical overview of subaqueous explosive volcanism. In: Explosive subaqueous volcanism (White, J.D.L.; Smellie, J.L. & Clague, D.A., Eds.), American Geophysical Union, Washington DC. Geophysical Monograph Series 140: 1–23. <https://doi.org/10.1029/140gm01>
- Ziegler, P.A. (1990). Geological Atlas of Western and Central Europe. Shell International Petroleum Maatschappij B.V., The Hague, 239 pp.